CHALMERS


# Modeling and simulation of cultivator load signals with a fatigue damage perspective

*Master's Thesis in Mathematical Statistics*

Xin Zhao

Department of Mathematical Science
*Division of Mathematical Statistics*
Chalmers University of Technology
Göteborg, Sweden 2011
Master's Thesis 2011:6

**Abstract**

In this paper a new stochastic process – Laplace moving average process(LMA) is used to simulate the load signals recorded from a stiff-structured cultivator machine while it is driven on the rough field. Fatigue damage estimation is the main focus of this thesis and rainflow cycle count method is used for this purpose. Gaussian process is used to simulate the tine vibration when it is not in the working state. The skewed load signals with random extreme values produced by working tines are simulated by the Laplace moving average process. As a very appropriate method to simulate loaded signal, it generates slightly-overestimated damage values, which is of great importance for successful machine designs. Furthermore, Monte Carlo study is used to evaluate the completeness and robustness of the LMA simulation. Later, variability analysis with bootstrap is applied to assess the difference of sample characteristics among different experiments. In the end, we investigate the correlation between loaded signals from different tines and signals corresponding to different physical properties. By principal component analysis, we evaluate the rainflow damage of a virtual synthetic signal with maximized variance. Suggestions for further simulation study are given in the end too.

**Keyword**: Laplace moving average, Laplace distribution, fatigue life prediction, rainflow cycle count, Monte Carlo, bootstrap

## Acknowledgment

I would like to thank my supervisor Mats Kvarnström and my examiner Igor Rychlik for their extensive help and warm encouragement during the last 6 months. As an unexperienced student newly entered the field of fatigue risk analysis, they gave me precious patience and efficient instructions, which are of great help in guiding me toward the right track. Also, I would like to thank Henrik Gunnarsson, the representative of the cooperating company Väderstad-Verken AB for his constant concern with the project and valuable suggestions in the meetings. Last but not least, I would like to thank Uno Nävert for introducing me to Fraunhofer-Chalmers Research Centre for my master thesis with such an exciting topic. It has been a great pleasure to work here.

Xin Zhao
Göteborg June 6th, 2011

# Contents

# 1 Introduction

Fatigue damage is a very important topic in industrial production as it is a major reason for material failure as noted by [1]. Usually in laboratory tests, oscillating stress signals with constant amplitudes are applied to the material specimen and the material is subject to repeated loading and unloading until it fractures. However in real world applications, the load signals frequently preserve the pattern of a stochastic process than constant amplitude sinusoids. For example for the road profile, due to the randomness of the rough surface, load responses it causes to the vehicle during driving can be modeled by a random process. Numerous studies have been carried out to model the road profile by means of Gaussian process as presented in [7]. But evidence was found in [3] that irregular sections that exists in the road profile are mainly responsible for the fatigue damage induced in vehicles. As a result, the stationary Gaussian process cannot give accurate modeling in fatigue application as the fatigue life prediction from Gaussian model may greatly overestimate the real life of an instrument. To compensate for such an insufficiency, Laplace moving average process is constructed to model road surface with extreme roughness as presented in [4].

In our project, we look for a suitable model to simulate the load response of a cultivator while it is working on rough lands. Data were collected from a cultivator prototype that has three tines attached to a frame. When the tine touches down into the ground, we call it loaded. Otherwise it is unloaded. The three tines are controlled individually so various combination of loading pattern can be recorded. Adapters attached to the conjunction of the tines with the frame measure all the forces and moments transferred from the tine to the framework. In our analysis, we focus on the simulation of the vertical load on individual tines and their combinations. Another important simplification is that the structure we consider in our model is a stiff structure. This has two important consequences. On the one hand the stresses are linear combinations of the external loads. On the other hand the stress is approximately proportional to the external load. The first point justifies the necessity of investigation of the load combinations while the second point greatly reduces the complexity of simulation and the corresponding damage estimation. In the forth coming we will show that the Gaussian process and the Laplace moving average process (LMA) will retain their characteristics when passing through a linear filter. So if Gaussian or LMA loads are acting on a linear structure, then local stresses which cause fatigue damage are Gaussian or LMA processes too and respectively equal to the load process multiplied by a constant. The constant depends on the structure's geometry, material and possible model errors. Since the goal of our paper is to find a simulation method that can generate load signals producing fatigue damage closest to the damage caused by the real load, the value of the constant we use is not important for this purpose. So in the following text we will not distinguish between the load and stress and build our analysis on the load data we have collected.

This thesis mainly consists of three parts. In the first part we summarize some important properties of the Gaussian process and LMA process and later use them to simulate unloaded load signal and loaded ones. The accuracy of models is evaluated

by means of Rice formula and fatigue approximation. Later we focus on the loaded signals and use Monte Carlo method to observe the generality of one simulated signal in capturing parametric properties of the original signals. We also study the variability of output characters among different experiments by means of bootstrap. In the last part we use principal component analysis to investigate the combined signals and the corresponding damage. Investigation of signals from other channels are included as well.

# 2 Data description

## 2.1 Cultivator protopye and descriptions of the experiment design

The analysis presented in this paper is based on a simplified version of a cultivator machine, which we call a cultivator prototype as shown in the photo in Figure 1. It has three tines attached to the front frame and the distance between each pair of two tines is one meter. Data on vibrations were collected when the cultivator was driven on the rough land in Rimstad with at constant speed. All combinations of the loading scenarios of the three tines regarding to different physical measurements are recorded. For each type of loading situation we repeat the experiment twice. When a tine is in the loaded state, it reached 10cm down into the ground and was dragged by the tractor to plough the field. Every round of the driving test with the loaded tine(s) consists of three sections in loaded state with a distance of 50 length units each and two sections of unloaded state with 20 length units per section. Figure 1 sketches the loading pattern of one driving cycle. The land was relatively soft with a lot of stones which cause the majority of damage when the cultivator hit on them.

Figure 1: Photo of the prototype model used in the experiment

Table 1: Sketch of the driving pattern of a loaded tine

| Position | starting | down | top | down | top | down | closing |
|---|---|---|---|---|---|---|---|
| Distance[length units] | 10 | 50 | 20 | 50 | 20 | 50 | 10 |

## 2.2 Signal data description

There are 16 data files containing two repetitions of each of the 8 kinds of loading scenarios. Each data file consists of 44 measurements of signals at 500Hz over roughly 2 minutes. Since the focus of our analysis is damage estimation from the vibration data, we only make use of 6 groups of data which respectively are named Fx, Fy, Fz, Mx, My and Mz representing force and momentum in $X$, $Y$ and $Z$ directions. Also, due to the nature of experiment design, each signal contains 3 parts corresponding to the time when the tine is lowered down into the ground; see the following Figure 2 obtained from Fy for a first impression.

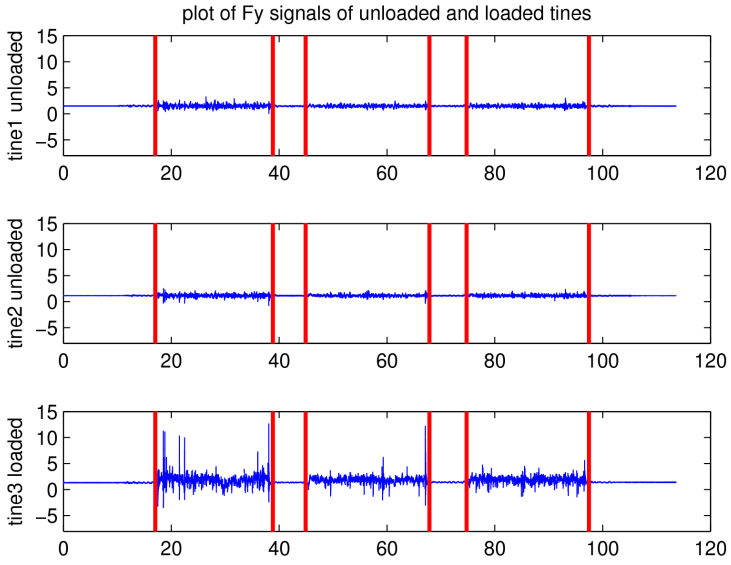


Figure 2: Signal plot of tines when unloaded and loaded

However, some of the data displays transient pattern which captures the moment when the tine hits the ground. The following Figure 3 of data Fz exposes such a property. Although the sudden force a tine receives when it hits the ground may contributes greatly to the fatigue of the material, to simplify the discussion here, from now on we will constrain ourselves to the stationary part and leave the damage analysis of the transient process to the further study. So in the following analysis, we cut off the transient vibration and investigate the relationship between the damage and the stationary vibration when the tine is in the ground. Among the 16 data files, 2 data files contain systematic errors so we have to drop them. Ultimately, we have in total 60 loaded signals and 66 unloaded signals.

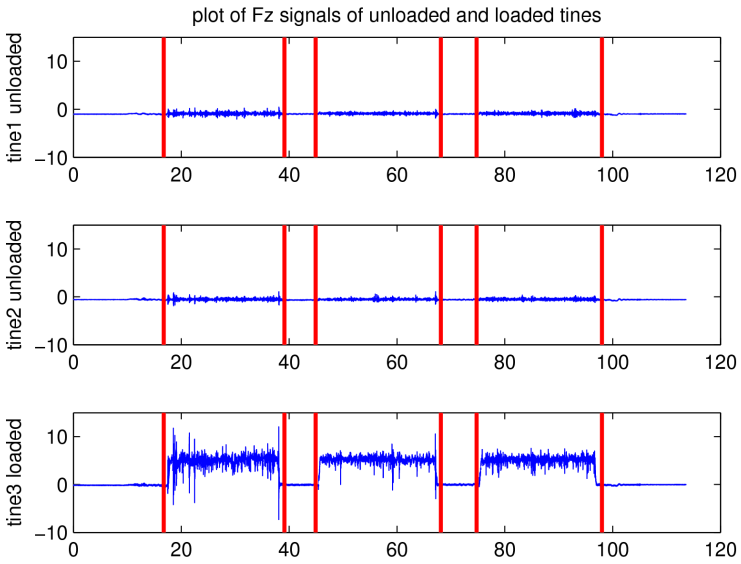


Figure 3: Signal plot of tines with transient pattern when unloaded and loaded. In the third figure, we can observe transient patterns in the beginning of each section of the vibration signal. An enlarged picture of the transient signal is shown in Figure 4.

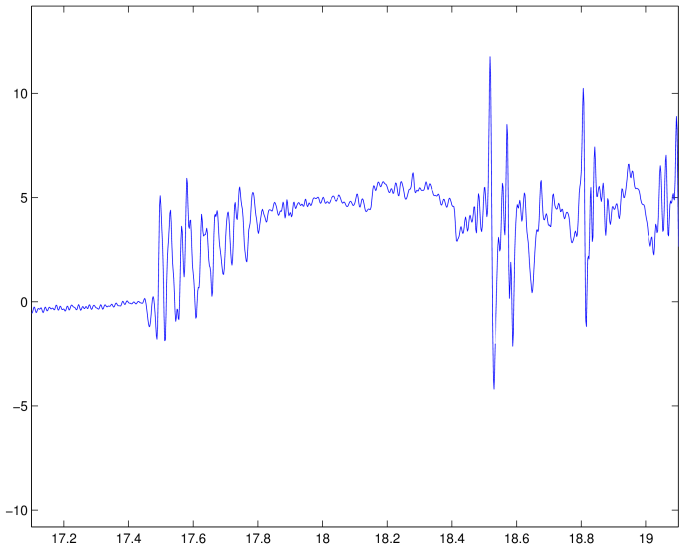


Figure 4: Transient part of Fz signal

# 3 Fatigue review

According to [1], Fatigue is a two-phase process starting with the initiation of microscopic cracks in the material, and in the second phase these cracks continue to grow to a critical size at which fracture occurs. During the progress, the material is subjected to repeated loading and unloading. Therefore it is natural to use the number of load cycles before failure to measure the material strength against fatigue. The traditional laboratory experiment of fatigue testing is carried out by applying oscillating stress cycles with constant amplitudes to a material component and observe the number of cycles it sustains before fracture. The specialty of the stress load having constant amplitudes means that each load has one local maximum and minimum per period. One commonly used stress function is a sinusoid function suggested by August Wöhler in 1870 which is written as:

$$x(t) = \frac{u+v}{2} + \frac{v-u}{2}\sin(\lambda t), t \geq 0 \tag{3.1}$$

where $v$ is the maximum of the cycle while $u$ is the minimum and $\lambda$ is the frequency. One can easily notice that $x(t)$ is a constant amplitude load. In experiments Wöhler found out that the number of periods to failure mainly depends on $v$ and $u$ and is insensitive to the frequency $\lambda$. When $v$ and $u$ are large, the shape of the stress function has comparatively less significant influence to the the number of cycles to failure. If the ratio between local maximum and minimum is kept constant, i.e., the ratio $\frac{u}{v}$ is kept constant and the range $s = v - u$ varies, one can obtain a so-called S-N curve that describes the log-linear relationship between the number of cycles to failure $n$ and the stress cycle range $s$ by regression with observed data. The function of the S-N curve is given by:

$$\ln(n) = a - k\ln(s) + e, \tag{3.2}$$

with constants $a > 0$, $k \geq 0$. They depend on material properties and the stress ratio $\frac{u}{v}$. The term $e$ follows a normal distribution $N(0, \sigma^2)$ and it includes the total error due to scatter in material, component properties and statistical errors.

If a load follows the stress function described by formula (3.1), during time interval $[0, t]$, there are $n_t = \frac{t\lambda}{2\pi}$ local maximums $v$ in the load. According to (3.2), the fatigue failure will occur when

$$\ln(n) - \ln(n_t) = a - k\ln(v-u) + e - \ln(n_t) = a + e - \ln(D(t)) < 0,$$

where $D(t) = n_t(v-u)^k$ describes the damage caused to a material. The greater $D(t)$ is, the easier the fatigue failure will happen. One should note that $D(t)$ is positively related to the number of cycles the material experiences in the test and the difference between the local minimum and maximum. When a more general form of regression line is used in the fatigue test with constant amplitude stress, instead of $v-u$, $D(t) = n_t f(u, v)$ and $f(u, v)$ is called the damage function. It it straightforward to see that $f(u, v)$ represents the damage accumulated per cycle.

However in real world, loads are more often random than constant amplitude sinusoids. Instead of having exactly one local maximum and minimum in each period, the pattern of extreme values of a load process might be irregular. Therefore we need to find an algorithm to search for local maximas and minimas in the stress and pair them up to construct a sequence of load cycles for damage calculation. This procedure is called cycle counting and various methods are developed for this. So far the most popular and most commonly used method is the rainflow cycle count introduced by Endo in 1967.

The rainflow count is meant to pair maxima and minima which are top and bottom of the closed hysteresis loop in the stress-strain path [8]. As shown in Figure 5, the hysteresis loop of hanging corresponds to a downward stress highlighted by the up-side-down triangle while the loop of standing corresponds to the upward stress emphasized by the gray triangle.

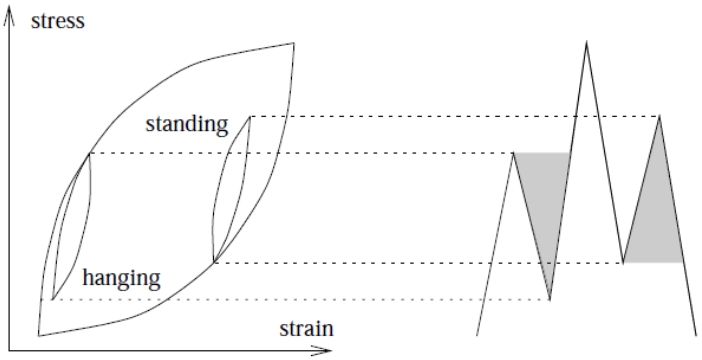


Figure 5: Hysteresis loops in the stress-strain plane

In this text, we use the definition of rainflow given by Rychlik in 1987 [10] from the perspective of statistical analysis.

**Definition 1** (Rainflow cycle count)**.** *In the rainflow cycle count, each local maximum of the load process is paired with one particular local minimum, determined as follows:*

1. *From the local maximum one determines the lowest values in forward and backward directions between the time point of the local maximum and the nearest points at which the load exceeds the value of the local maximum.(Figure 6)*

2. *The greater of those two minimum values is the rainflow minimum paired with that specific local maximum, i.e. the rainflow minimum is that which falls the least before reaching the value of the local maximum again on either side.*

3. *The cycle range, s, is the difference between the local maximum and the paired rainflow minimum.*

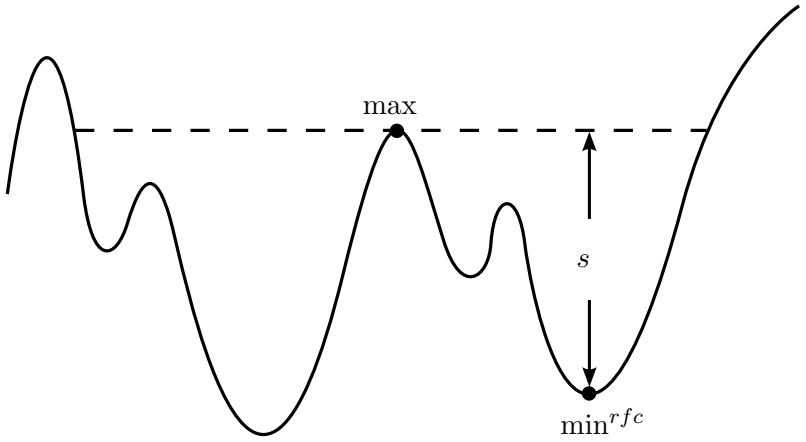


Figure 6: A rainflow pair

In our analysis of the cultivator load data, while counting the rainflow cycle, we make use of the so-called *4-points algorithm* which we also present here:

**Definition 2** (The 4-points algorithm)**.** *First one finds the sequence of turning points in the load. The sequence is denoted by $x_i$, for $i = 1, ..., n$. A stack of 4 points is used. It is initialized with the first 4 points of the signal $s = [s1 = x1, s2 = x2, s3 = x3, s4 = x4]$. The residual vector $r = [r1, ..., rm]$, with length $m$ is empty, i.e. $m = 0$.*

- *The rainflow cycles and the residual are identified by applying the following counting rule:*

  ***(c)*** *If $min(s1, s4) \leq min(s2, s3)$ and $max(s2, s3) \leq max(s1, s4)$, then the pair $(s2, s3)$ is a cycle, that is if the interval spanned by the inner points of the stack is contained in the interval spanned by the corners of the stack.*

- *If this is the case, i.e. condition (c) holds, the cycle $(s2, s3)$ is counted and both points deleted from the stack. Now the stack has to be refilled. If possible the stack is filled with points from the past, that is from the residual. In detail this means ($k$ denotes the next point of the signal $x$):* ***(r1)*** *If $m = 0$, then $[s1 = s1, s2 = s4, s3 = xk, s4 = xk + 1]$, and $k = k + 2$.*

  ***(r2)*** *if $m = 1$, then $[s1 = rm, s2 = s1, s3 = s4, s4 = xk]$, $k = k + 1$ and $m = 0$.*

  ***(r3)*** *if $m \geq 2$, then $[s1 = rm - 1, s2 = rm, s3 = s1, s4 = s4]$, and $m = m - 2$.*

  *Then the counting rule is applied again, i.e. go to (c).*

- *If the counting condition (c) is not fulfilled, then*

  ***(r4)*** *$m = m + 1$, $rm = s1$, $[s1 = s2, s2 = s3, s3 = s4, s4 = xk]$, and $k = k + 1$, and go to (c).*

*This is repeated until the last point of the time signal is reached and (c) does not apply any more. The result of this procedure is the sequence of turning points, tops and bottoms*

*of closed cycles, and the residual $r_j$, $j = 1, ..., m$, containing the remaining sequence of turning points.*

Due to its ability to capture the nature of material fracture process, the rainflow method has been widely accepted as the best cycle counting procedure to date and has become the industrial de facto standard [10].

Employing the idea of linear accumulation, Palmgren-Miner rule gives us an indication of damage calculation with more complicated loads scenarios. The Palmgren-Miner linear damage hypothesis states that when a material experiences random loads, the number of cycles to failure is equal to the sum of cycles contributed by each kind of stress magnitude, i.e., if there are $m$ kinds of loads with difference stress magnitudes in a spectrum, the total number of cycles to failure is given by: $N(t) \equiv \sum_{i=1}^{m} n_i(t)$ where $n_i(t)$ is the cycles to fatigue contributed by stress level $i$. Since the rainflow method provides us with a sequence of organized cycles $(u_i, v_i)$, $i = 1, \cdots, N(t)$ and the damage function $f(u_i, v_i)$ describes the amount of damage taken per cycle, the damage accumulation of a load process is written as

$$D(T) = \sum_i f(u_i^{rfc}, v_i^{rfc}) + D^{res} \tag{3.3}$$

where $D^{res}$ denotes extracted cycles from the residuals calculated by $r_j$, $j = 1, \cdots, m$ as in Definition 2. Frequently the damage function $f(u_i, v_i) = (v_i - u_i)^k$ is used as an approximation when $\frac{v_i}{u_i}$ is constant. The exponent $k$ is a material and load related value that can vary between 1 to 6. For the fatigue caused by road roughness, $k$ roughly equals to 3. In our analysis we will use the same value, i.e., our damage function is $f(u_i, v_i) = (v_i - u_i)^3$. Evidence of the efficiency of Palmgren-Miner rule in the damage estimation by rainflow cycle counting can be found in Jono [6] in experiments with plastic strain.

Although the rainflow counting method can give accurate life prediction, sometimes some other counting method might be more convenient to use when the measurements are not available or loads acting on a component are defined indirectly. The two ways we would like to mention before we close this section are the min-max cycle count and the crossing count as they serve as a lower and upper bound for the value obtained by the rainflow method for life prediction. To be more specific, for any load the equivalent range computed using rainflow cycle counts is bounded from below by the equivalent range computed by min-max cycles and from above by crossing cycle counts. The min-max count pairs the local maximum with its preceeding minimum. The definition of the crossing count method makes use of the term *level crossing spectrum* which we first give:

**Definition 3.** *The level crossing spectrum $N^+(u)$ is the number of times the load upcorsses the load level $u$. If $x(t)$ represents the load signal, $N^+(u)$ is define as*

$$N^+(u) = \#\tau \in [0, t] : x(\tau) = u, \dot{x}(\tau) > 0.$$

The importance of the level crossing spectrum is that it presents a general look of the distribution of the signal crossing schemes over its range alike to a histogram of

the number of crossings with respect to different intensity levels. Due to its descriptive property, it is frequently used for comparison of different signals. We detail on its usage in section 4.1. Now we give the definition of the crossing cycle count [9].

**Definition 4** (crossing cycle count)**.** *The crossing cycle count* $\boldsymbol{C}$ *is a collection of all pairs* $(u_i, v_i)$ *in* $C_u$ *when* $u$ *takes values* $0, 1, \cdots$.

$$\boldsymbol{C}=C_0 \cup C_1 \cup C_2 \cup \cdots,$$

*where* $C_u$ *are defined as*

$$C_u := \{(u_i, v_i) : N^+(u_i) \leq u, N^+(v_i) \leq u \text{ and } N^+(z) > u \text{ for all } z \in (u_i, v_i)\}.$$

*Elements in* $\boldsymbol{C}$ *will be called crossing cycle counts.*

# 4 Univariate signal modeling

The main tool for signal modeling is spectral theory. A term we will frequently use in the following context is spectral density. Simply speaking, spectral density tells the distribution of frequencies in the signal. Since the stochastic vibration process we consider here is stationary, which means the statistics of the process do not change with time, the spectral density we will make use of in our discussion is a power spectral density (PSD). Without further statement, the process we consider in our discussion is assumed to be a zero mean process. First we give the definition of spectral density.

**Definition 5** (Power spectral density of a random process)**.** *The PSD $S_z(\omega)$ of a weak stationary random process $z(t)$ is the Fourier transform of its autocorrelation function $R_z(\tau)$:*

$$S_z(\omega) = \frac{1}{2\pi}\int_{-\infty}^{+\infty} R_z(\tau)e^{-i\omega\tau}d\tau \tag{4.1}$$

$$R_z(\tau) = \int_{-\infty}^{+\infty} S_z(\omega)e^{i\omega\tau}d\omega \tag{4.2}$$

where the autocorrelation function of a stochastic process is defined as the ensemble average

$$R_z(\tau) = \mathrm{E}[z(t)z(t+\tau)] \tag{4.3}$$

which for ergodic processes can be computed by the following time average:

$$R_z(\tau) = \lim_{N\to\infty}\frac{1}{N}\sum_{i=1}^{N} Z(t_i)Z(t_i+\tau) \tag{4.4}$$

By this, we can write $S_z(\omega) = F\{R_z(\tau)\}(\omega)$.

When the random signal $z(t)$ is applied to a linear time-invariant (LTI) system with a unit impulse response $h(t)$, the input and output relationship is given by:

$$y(t) = z(t) * h(t) = \int_{-\infty}^{+\infty} h(t-u)z(u)du \tag{4.5}$$

where $y(t)$ is the output signal. The operator $*$ denotes the convolution. Let $Y(\omega)$ be the Fourier transform of $y(t)$, $Z(\omega)$ be the Fourier transform of $z(t)$ and $H(\omega)$ be the Fourier transform of $h(t)$, i.e.,

$$y(t) \Longleftrightarrow Y(\omega) \quad Z(t) \Longleftrightarrow Z(\omega) \quad h(t) \Longleftrightarrow H(\omega),$$

then according to the time convolution property, the equality

$$Y(\omega) = Z(\omega)H(\omega) \tag{4.6}$$

holds.

Since the energy spectral density (ESD) of a signal is defined as the square of its absolute spectral-domain specification, by squaring the absolute value of both sides of (4.6) we obtain that

$$\Psi_y(\omega) = |Y(\omega)|^2 = |H(\omega)|^2 |Z(\omega)|^2 = |H(\omega)|^2 \Psi_z(\omega). \tag{4.7}$$

where $\Psi_y$ and $\Psi_z$ represents the ESD of the output and input signals. Furthermore, as the PSD is plainly a time average of ESDs, the relationship between the input and output PSD of a LTI system can be easily derived from the (4.7) as

$$S_y(\omega) = |H(\omega)|^2 S_z(\omega) \tag{4.8}$$

This formula will be of great use when we calculate the kernel function of a convolution. Further examples will be given in Section 4.3 when the Laplace moving average process is introduced.

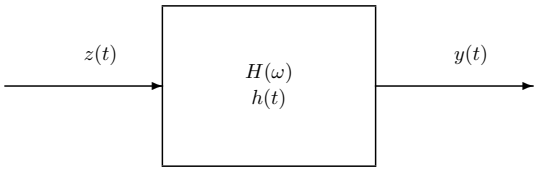


Figure 7: Transmission of a random process through a LTI system

In the following sections, we will use the term spectral density to denote power spectral density for the sake of simplicity. First we introduce a very useful function called Rice formula to observe the similarity of the data distribution to a Gaussian one. Afterwards, we present some fundamental properties of Gaussian process and LMA process, which respectively gives close representation of the unloaded and loaded signals.

## 4.1 Rice formula and spectrum of the loaded and unloaded data

A Gaussian process is a stochastic process for which any finite linear combination of the sample functions will be normally distributed. Inheriting from nice mathematical properties, Gaussian process has its great convenience in modeling vibrations of second order moments. In our case, when the tines are not loaded, as there are no input forces from the environment, the vibration happening to each of them is stable and induces the usage of Gaussian process in modeling. Recall that in Section 3, we mentioned that the level crossing spectrum describes the distribution of the signal crossing schemes over the range of the signal. It is used to access if a given process is suitable to model a certain signal. When a signal is a Gaussian process, Rice formula gives an analytical expression

of the expected number of crossings with respect to its levels. Referring to the detailed explanation in Section A of the Appendix, we see that for a Gaussian load, its expected number of crossings of a given level is a function of that level. So we have a one to one correspondence of the level to the expected number of crossings. WAFO package provides the algorithms to calculate the empirical crossings, by which we can plot the level crossing spectrum of different load data together with the line representing Rice formula to examine if a load follows a Gaussian distribution or not.

We use a level crossing plot to examine the distribution of unloaded data to see if they follow a Gaussian process. We notice that with different extents of similarity to Gaussian, the unloaded signals are in general non-Gaussian. To save the space of illustration, here we only use the test result of the unloaded tine 1 section 2 of file `CS80-0-0-10-01` as an example to show the crossing pattern. In figure 8, the solid red line represents the Rice formula and the dashed red line is a Gaussian signal simulated from the unloaded data. We plot the empirical crossing performance of the original data in two variants. The blue line depicts the crossing of the complete data while the green line corresponds to the crossings of data after the frequencies above $\frac{600}{2\pi}$ are filtered away. On both sides, the unloaded signal has fatter tails than a Gaussian process which indicates that the unloaded signal contains more extreme values than the a Gaussian process. Furthermore, the discrepancy of crossings being greater on the right tail than the left one tells that the signal tends to have extreme values more frequently in the positive direction than in the negative one. The same characteristic is observed in the normal probability plot in Figure 9.

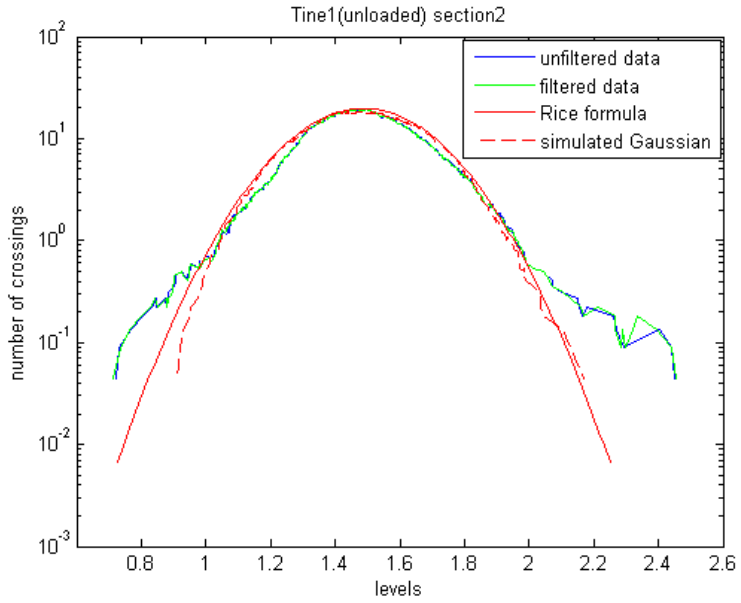


Figure 8: Comparison of the Rice formula and the level crossing of the unloaded tine 1 from section 2 repetition 1 in data `CS80-0-0-10-01`. Although crossings between level 1 and 2 follow a Gaussian process very well, we notice that the signal has much larger tails on both sides than a Gaussian process.

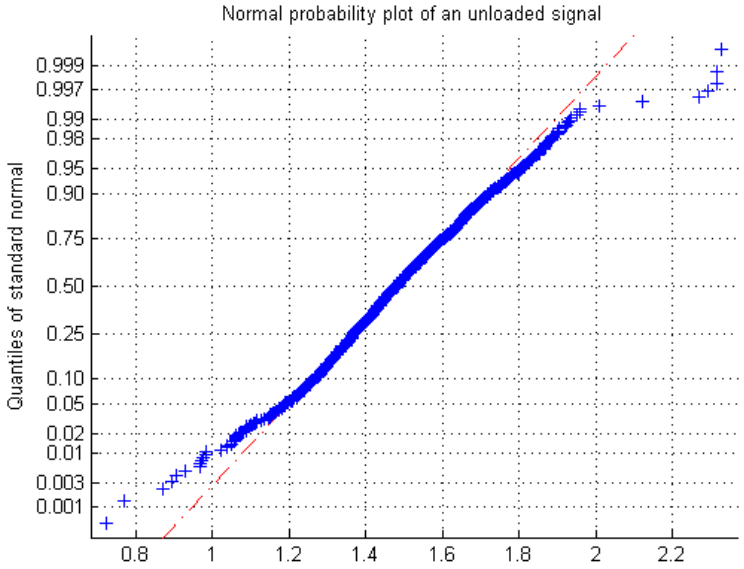


Figure 9: Normality test of the unloaded data from tine 1 section 2 repetition 1 in data `CS80-0-0-10-01`. Obvious disagreement between sample process values and the Gaussian distribution is displayed on both ends of the plot. This corresponds to the observation of fat tails in Figure 8 showing that the sample data has higher crossing density than a Gaussian process on both sides.

The objective of removing high frequencies is to reduce the upper bound of the damage estimation. We have known from Section 3 that the level crossing spectrum presents the upper bound of the rainflow damage estimation. As presented in (A.1) and (A.8), for a process $X(t)$, its variance and the variance of its derivative can be expressed by the spectral moments in the zeroth and second order:

$$\mathrm{Var}[Z(t)] = \int S(\omega)d\omega = \lambda_0 \tag{4.9}$$

$$\mathrm{Var}[\dot{Z}(t)] = \int \omega^2 S(\omega)d\omega = \lambda_2. \tag{4.10}$$

When the high frequency is cut off, this will have almost no influence on the variance of the process $\lambda_0$ while the variance of the derivative process $\lambda_2$ will decrease a lot more. As a result, the number of mean upcrossings will become smaller which will make upper bound of the rainflow damage estimation less conservative.

But here we notice that in our case the energy in the high frequencies is not sufficient to change the crossing pattern as the difference between the green line and the blue line is trivial. So in the rest of analysis we will base our study on the unfiltered original data.

In the same way, we look at the crossing intensity of the loaded signal from data of tine 3 section 1 in `CS80-0-0-10-01`. We can see in Figure 10 that this time the loaded signal has larger variability and deviates even more from the Gaussian load. The fatter right tail is reflected in the normal probability plot in Figure 11 at the right upper end. We notice that compared to Figure 9, the loaded signal shows more obvious deviation from Gaussian process. Figure 10 also gives us important clues about the critical model qualities we need to capture for a successful modeling of the loaded signal. Detailed explanations will be given in Section 4.3.

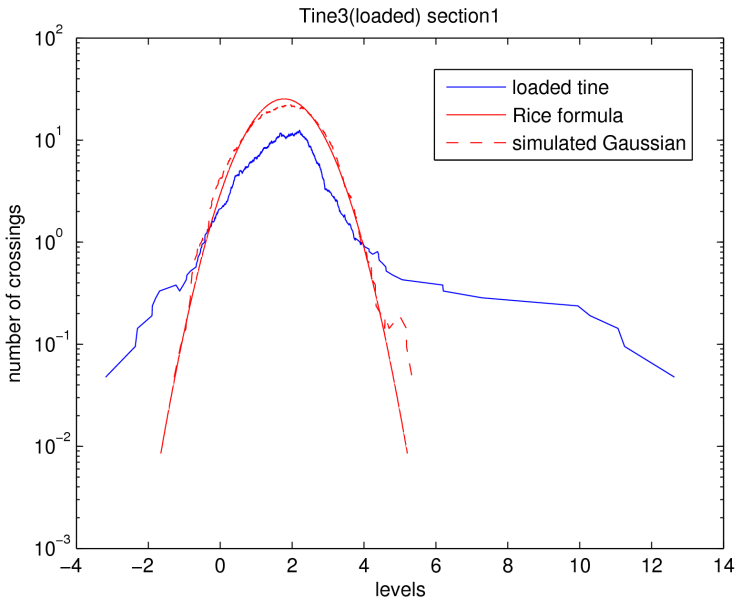


Figure 10: Comparison of the Rice formula and the level crossing of the loaded data of tine 3 from section 1 repetition 1 of data `CS80-0-0-10-01`. Compared with Figure 8, the loaded signal is significantly non-Gaussian and has substantially bigger tails than the unloaded signal.

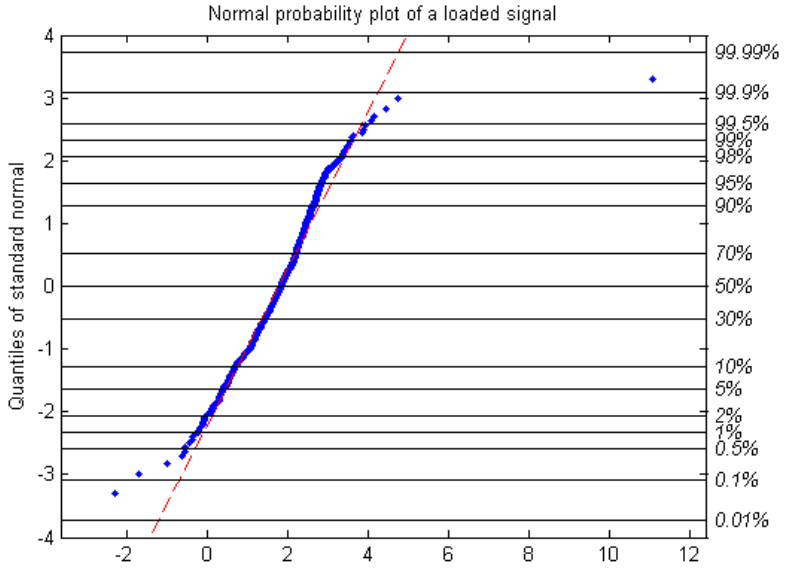


Figure 11: Normality test of the an unloaded data from tine 3 section 1 repetition 1 in data `CS80-0-0-10-01`. We notice that on both ends the loaded data has obvious disagreement with a Gaussian distribution.

Figure 12 is an example of the spectral density of an unloaded tine 1 section 1 to 3 from the data file `CS80-0-0-10-01` including the cut-off frequency. Compared to the spectral density shown in Figure 13 of a loaded tine 3 section 1 to 3 from data `CS80-0-0-10-01`, the unloaded signals have considerable less variance than the loaded signals, shown by the area of the spectral densities. In figure 12, the unloaded spectral density has exceptional high energy around frequency 380(radians), but the loaded signals do not have any spikes. Since spectral density uniquely decides the kernel function used to simulate a signal, great variability between spectral densities suggests the necessity of using different kernel functions. In either figure, the three spectral densities of the three sections follow almost the same pattern. But the patterns differer between loaded and unloaded scenarios.

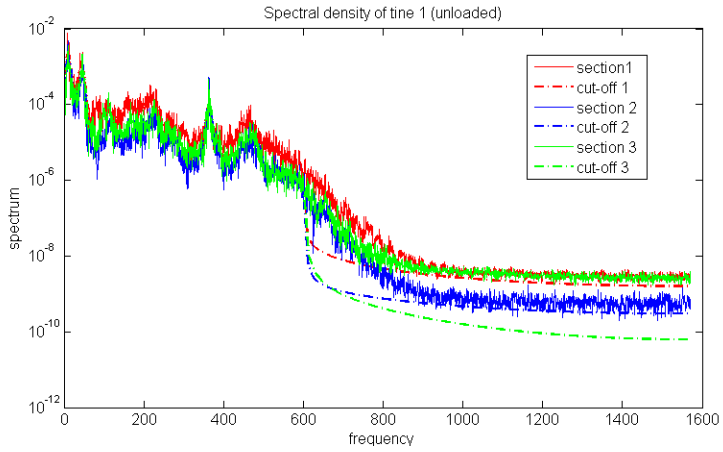


Figure 12: Spectral density of the three sections of tine one while unloaded. The cut-off of high frequencies are shown as dashed line. All three spectral densities follow almost the same pattern. A spike exists around frequency 380 (radians) indicating exceptional high energy around that particular frequency.

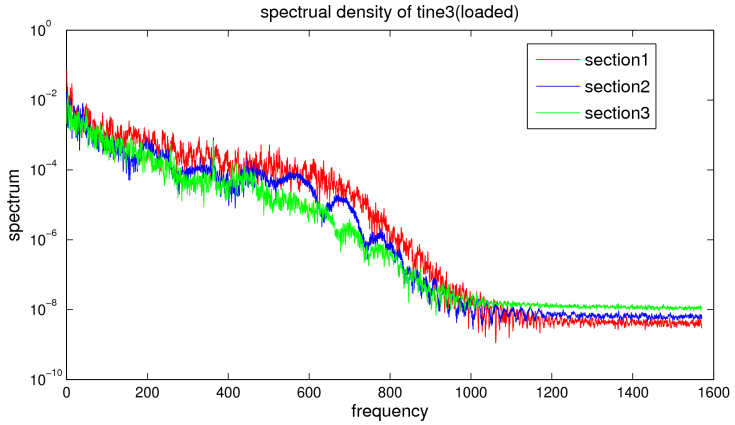


Figure 13: Spectral density of the three sections of tine three while loaded. Slight variability shows up between 400 (radians) and 800 (radians) among three spectral densities. In general they have homogeneous forms.

## 4.2 Modeling of the unloaded signal by Gaussian process

Although Gaussian process does not capture the complete characteristics of the unloaded signals, it still resembles a big part of the properties of the unloaded data so it serves as one possible way to simulate unloaded vibrations. Also since the damage of unloaded signals is negligible compared to the loaded ones, we give the focus of our study

to the simulation of loaded signals. Some underestimation of damage when modeling with Gaussian process is within our acceptance. One common way used to construct a stochastic output signal is by convolution. By convoluting a kernel function with a Brownian motion, we can generate a Gaussian process. That is, we set:

$$Z(t) = \int_{-\infty}^{+\infty} f(t-u)dB(u) \tag{4.11}$$

where $B(u)$ is a Brownian motion. In simulation, $B(u)$ is generated by $N_i\sqrt{dt}$ in which $N_i$ is a standard normal distribution and $dt$ is the time increment one chooses. So formula (4.11) can be approximated by

$$Z(t) = \int_{-\infty}^{+\infty} f(t-u)dB(u) \approx \sum_i f(x-x_i)N_i\sqrt{dx}. \tag{4.12}$$

As the convolution is simply a linear transform of the input signal, according to (4.8) and the fact that the spectral density of a Brownian motion is one, we have

$$S_Z(\omega) = \frac{1}{2\pi}|F\{f(\omega)\}|^2 S_B(\omega) = \frac{1}{2\pi}|F\{f(\omega)\}|^2. \tag{4.13}$$

So the kernel of a Gaussian function can be approximated by

$$f(\omega) = F^{-1}\{\sqrt{2\pi S_Z(\omega)}\}, \tag{4.14}$$

and $S_z$ can be obtained by Fourier transform of the autocorrelation function of the unloaded data.

By using the above logic, one can generate a simulated Gaussian process with the WAFO toolbox. To show the simulation result, we plot both, the unloaded data from tine 1 section 2 in data file `CS80-0-0-0-01` and its Gaussian simulated output in Figure 14. In the figure, we leave out the transient part in the beginning of the signal. Although the simulated Gaussian signal in red is a random sample of simulation and varies from one time to another, we still can see from this Gaussian simulation sample that it conserves less extreme values than the sample signal in blue. This observation corresponds to a fat tail in the crossing intensity in Figure 8.

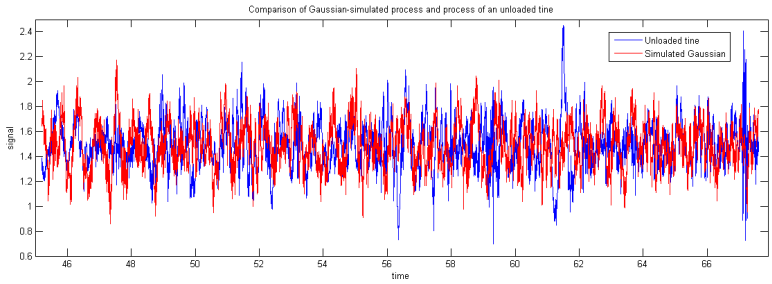


Figure 14: Plot of a signal from an unloaded tine and its Gaussian simulation. One can see from the figure that the simulated Gaussian conserves less extreme values in both positive and negative directions than the sample data.

Since loads at the extreme level will cause great damage, we can expect that the Gaussian simulated signal will have less expected damage than the value of the original signal. In the WAFO toolbox, the function $tp2rfc$ calculates the rainflow cycles from the sequence of turning points and produces output in the first column the sequence of rainflow minimums and in the second column the paired rainflow maximums. We can use the function

$$f(u, v) = (v - u)^k \tag{4.15}$$

to compute the damage where $v$ indicates the maximums and $u$ stands for the minimums. However if we have known that the waves follow a zero-mean stationary Gaussian process, it's convenient to introduce two terms: the significant amplitude $h_s$ and the frequency of mean level up-crossings(also called the apparent frequency) $f_z$ in order to approximate the rainflow damage. Continuing from the Rice formula (A.17), we define $h_s = 4\sqrt{\lambda_0}$ and $f_z = \frac{1}{2}\,\mathrm{E}[N(0)] = \frac{1}{2\pi}\sqrt{\frac{\lambda_2}{\lambda_0}}$. Then a crude approximation for the expected rainflow damage is

$$\mathrm{E}[D^{rfc}(t)] \approx 0.5 t f_z h_s^k.$$

## 4.3 Modeling of the loaded signal and LMA process

Observing from the crossing spectrum figure of the loaded tine in Figure 10, we notice that there are high crossing times over extremely high levels and more often than not, the number of crossings over high levels is greater than the number of crossings over the low levels. This indicates us to use a process preserving a lot of extreme values and mostly in the positive direction for an appropriate simulation. As a result the simulated loaded signal must have its vibration pattern displaying significant jumps, mainly, toward up-going direction. This phenomenon is easy to understand considering the resistance from the soil or hard rocks received by the tine when it hits on them in movement. When it meets especially hard rocks, jumps with huge amplitude are observed in the vibration signal. So Gaussian process is no longer suitable to simulate such an effect due to its insufficient generation of higher moments. Figure 15 shows the discrepancy between a loaded signal and the corresponding simulated Gaussian process from data `CS80-10-10-10-01` tine 3 section 2. We notice from the figure that Gaussian process cannot reproduce occasional jumps that come along with the loaded data.

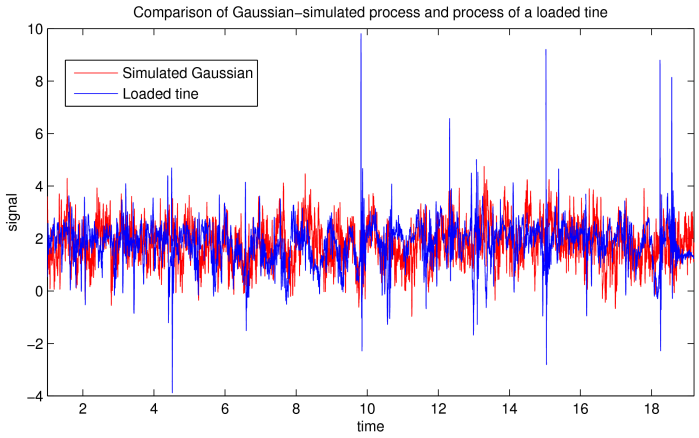


Figure 15: Plot of a signal from a loaded tine and its Gaussian simulation. One notices that Gaussian process is unable to capture the high jumps and skewness of the loaded signal.

Laplace moving average (LMA) is therefore introduced as a counterpart of the Gaussian process with increased parametric freedoms including the skewness and kurtosis, which are of great help to capture the asymmetry effect and the extreme values. We construct a Laplace moving average output signal in the same way as shown in Section 4.2, that is, by means of convolution. But instead of a Brownian motion, we convolute the kernel function with a Laplace motion. So the equation (4.11) in Section 4.1 now changes into:

$$Z(t) = \int_{-\infty}^{+\infty} f(t-u)d\Lambda(u) \tag{4.16}$$

where $\Lambda(u)$ is a Laplace motion, whose definition is given below:

**Definition 6** (Laplace motion)**.** *A Laplace motion $\Lambda(t)$ with the asymmetry parameter $\mu$, the space scale parameter $\sigma$ and the time scale parameter $\nu$, $LM(\mu, \sigma, \nu)$ is defined by the following conditions:*

- *it starts at the origin, i.e., $\Lambda(0) = 0$;*
- *it has independent and stationary increments;*
- *the increments by the time scale unit have a symmetric Laplace distribution with the parameter $\sigma$, i.e.,*

$$\Lambda(t+\nu) - \Lambda(t) \overset{d}{=} Laplace(\mu, \sigma)$$

*If $\mu = 0$, $\sigma = 1$ and $\nu = 1$, the process $\Lambda(t)$ is called the standard Laplace motion.*

During the simulation, the increments of the Laplace motion — being Laplace distributed — are generated by $N_i\sqrt{\nu\Gamma_i}$ where $\Gamma_i$ represents a Gamma distribution with shape parameter $dx/\nu$ and scale parameter 1 and $N_i$ is a standard normal distribution. So formula (4.16) can be approximated by

$$Z(x) = \int f(x-u)d\Lambda(u) = \sum f(x-x_i)N_i\sqrt{\nu\Gamma_i}. \tag{4.17}$$

We notice that the variance of the increment $N_i\sqrt{\nu\Gamma_i}$ equals to the interval of time elapsed:

$$\begin{aligned}
\mathrm{Var}(N_i\sqrt{\gamma\Gamma_i}) &= \mathrm{Var}(N_i)[\mathrm{E}(\sqrt{\gamma\Gamma_i})]^2 + \mathrm{Var}(\sqrt{\gamma\Gamma_i})[\mathrm{E}(N_i)]^2 \\
&\quad + \mathrm{Var}(N_i)\,\mathrm{Var}(\sqrt{\gamma\Gamma_i}) \\
&= (\mathrm{E}[\sqrt{\gamma\Gamma_i}])^2 + \mathrm{Var}(\sqrt{\gamma\Gamma_i}) \\
&= (\mathrm{E}[\sqrt{\gamma\Gamma_i}])^2 + \mathrm{E}(\gamma\Gamma_i) - (\mathrm{E}[\sqrt{\gamma\Gamma_i}])^2 \\
&= \mathrm{E}(\gamma\Gamma_i) = dx.
\end{aligned}$$

A Laplace motion made up by a train of such increments is sometimes written as $B(\Gamma(x))$ where $B(t)$ is a Brownian motion. This simply comes from the fact that a Laplace process is constructed by modified Brownian motion whose variance of each increment follows a Gamma distribution.

However in the practical data fitting procedure, in order to generate a zero mean process, we need to introduce a drift term to adjust the mean value of the process. Therefore we apply a more generalized version of the LMA process given by:

$$\Lambda(x) = \gamma x + \mu\Gamma(x) + B(\Gamma(x)) \tag{4.18}$$

and parameters include the asymmetric Laplace distribution parameters $\mu$, $\sigma$, $\nu$, the drift $\gamma$ and the kernel function. Those the components to estimate based on the four moments of the data and its spectral density. The parameter $\nu$ can be used to scale the kernel function $f$. So for convenience we use the normalized kernel by assuming $\int f^2 d = 1$. Most of the time estimating the kernel function is not a easy task to do, however since in our experiment, the driving direction does not influence the vibration signal, i.e., driving in one direction and in its opposite direction have the same stochastic signal, the kernel function we consider is symmetric and therefore it has such a form with respect to the spectral density $S_z$:

$$S_z(\omega) = \frac{1}{2\pi}|F\{f(\omega)\}|^2. \tag{4.19}$$

The estimated kernel function calculated from average spectral density is depicted in Figure 16. As we expect, the kernel function is symmetric.

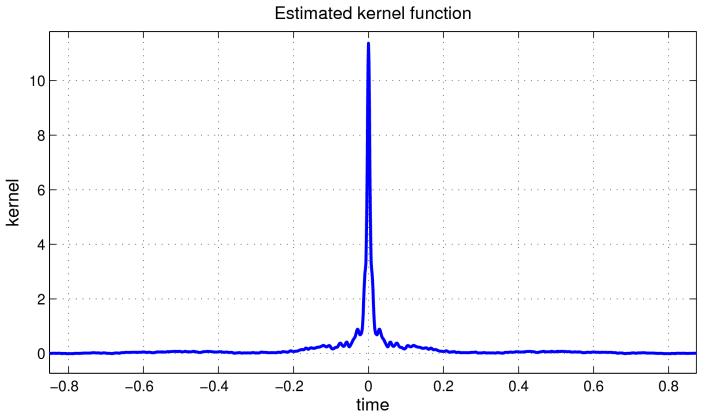


Figure 16: Estimated kernel function obtained from the average spectral density

As the spectral density can be calculated from the data in WAFO by *dat2spec*, the kernel function is easily obtained by inverse Fourier transform. Recalling that different from a Gaussian process, the LMA process has non-zero third and forth moments, the rest of the parameters $\mu$, $\sigma$, $\nu$ and $\gamma$ are obtained by fitting into first to forth moments of the stochastic process. The mean, variance, skewness and excessive kurtosis are straightforwardly accessible from data and we can approximate the parameters by means of following formula once the kernel function is obtained by 4.19 [2]:

$$\mathrm{E}[Z(x)] = (\gamma + \frac{\mu}{\nu}) \int f(x)dx, \tag{4.20}$$

$$\mathrm{Var}[z(x)] = (\mu^2 + \sigma^2) \int f(x)^2 dx, \tag{4.21}$$

$$\mathrm{Skew} = \mu\nu^{1/2} \frac{2\mu^2 + 3\sigma^2}{(\mu^2 + \sigma^2)^{3/2}} \frac{\int_{-\infty}^{+\infty} f^3(x)dx}{(\int_{-\infty}^{+\infty} f^3(x)dx)^{3/2}}, \tag{4.22}$$

$$\mathrm{Kurt} = 3\nu \left(2 - \frac{\sigma^4}{(\mu^2 + \sigma^2)^2}\right) \frac{\int_{-\infty}^{+\infty} f^4(x)dx}{(\int_{-\infty}^{+\infty} f^2(x)dx)^2}. \tag{4.23}$$

After we have obtained an estimate for these parameters, we can generate an LMA process by the algorithms given in Appendix B. In Figure 17 we can see that the simulated LMA process can produce large jumps and phases with higher positive values than negative ones. The simulated LMA process captures the characteristics of loaded data from the file `CS80-10-10-10-01` tine 3 section 2 very well.

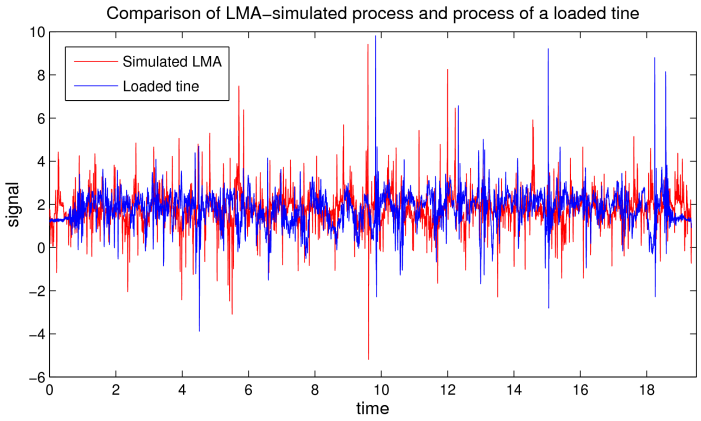


Figure 17: Plot of a signal from a loaded tine and its LMA simulation. We can see that LMA in red captures the skewness and extreme values that exist in the original data in blue very well.

A convenient property of the LMA process is that if it passes through a linear filter, the output is still an LMA process. Denote $h(x)$ as the impulse response of a linear filter. Then

$$h * Z(t) = \int h(t-x)Z(x)dx = \int\int h(t-x)f(x-u)d\Lambda(u)dx \tag{4.24}$$

$$= \int \left( \int h(t-x)f(x-u)dx \right) d\Lambda(u) = \int h * f(t-u)d\Lambda(u) \tag{4.25}$$

So if one feeds an LMA process with kernel $f$ into a system with impulse response $h$, the output signal is still an LMA process, but with kernel $h * f$.

From the vibration signal data, we can directly estimate the damage by means of the rainflow method. To simplify the procedure of damage calculation, we define a function *computeDamage* with input arguments including the signal data as the first component and the damage coefficient $k$ as the second one. $k$ varies according to the material we consider and in our situation, $k$ is set to be 3. Calculating with data of tine 3 section 2 in `CS-10-10-10-01`, we obtained the damage estimation of both simulated Gaussian process and LMA process of a loaded signal and the result is presented in the following table:

Table 2: Comparison of damage estimation of Gaussian simulation and LMA simulation. We can see that LMA captures the fatigue damage property of the original data very well however Gaussian process underestimates damage values to just half of the true damage.

| Estimated damage | Data | LMA | Gaussian simulated |
|---|---|---|---|
| | 1174 | 965.5 | 419.4 |

The comparison of the first four moments of simulated Gaussian process and simulated LMA process is given in Table 3.

Table 3: Comparison of the estimated moments of the Gaussian simulation and the LMA simulation. We can see that LMA captures the kurtosis of the original data accurately while the kurtosis of Gaussian process underestimated by a factor of more than three.

| Moment | 1 | 2 | 3 | 4 |
|---|---|---|---|---|
| Data | 1.7879 | 0.7835 | 0.0994 | 10.0500 |
| LMA | 1.8675 | 0.7743 | 0.0719 | 9.5995 |
| Gaussian simulated | 1.7879 | 0.7750 | 0.0221 | 2.9843 |

We notice that the LMA-simulated signal yields both estimated damage and moment values extremely close to the corresponding values of the real vibration signal. This justifies our guess that LMA serves as a good way to simulate loaded data. However, before we give our affirmative conclusion, we need to test the robustness of LMA simulation to see if it constantly shows good reproduction of the loaded signal properties when the number of simulation times increases. For this purpose, a Monte Carlo test in the next section.

# 5 Monte Carlo study of simulated loads

## 5.1 Monte Carlo study on single loaded signal

In order to evaluate the quality of a simulation algorithm, we compare the statistics obtained from the simulated signals to those calculated from original signals. If the simulation method is reliable, we will have high similarity between these values. Since damage estimation is the focus of this thesis, we will use it as a major criteria to evaluate the quality of the simulation. We use Monte Carlo study to investigate the empirical distribution of the moments and damage estimation obtained from the previous step of simulation and compare it to the original signals. This approach involves the following three steps:

1. Compute the spectral density, the first to forth moments and estimated damage from one signal process.

2. Use above results as inputs to simulate an LMA process by the method proposed in Section 4.3.

3. Repeat step 2 for N times to generate N simulated-LMA processes. Calculate its moments and estimated damage for each of these N simulations and observe the empirical distribution by plotting histograms of the groups of damage values and moment values.

In the Figures 18 to 20, we show the result of the Monte Carlo study of a loaded tine 3 section 3 from data `CS80-10-10-10-02`. The histogram is generated based on 1000 simulated signals using the same parameters calculated from the original data which is represented by the red line. One can see the LMA simulation generates signals producing higher damage than the corresponding value of the real data. The distribution of kurtosis is shown in Figure 19, but the overestimation is not obvious. Looking through all the kurtosis distributions, we notice that it is in general slenderly overestimated. The empirical density that shows both of these two values being over-estimated is no coincidence. Since higher kurtosis indicates exceptional extreme values, in return they produce bigger rainflow estimation of damage. The simulated skewness in Figure 20 appears to be unbiased.

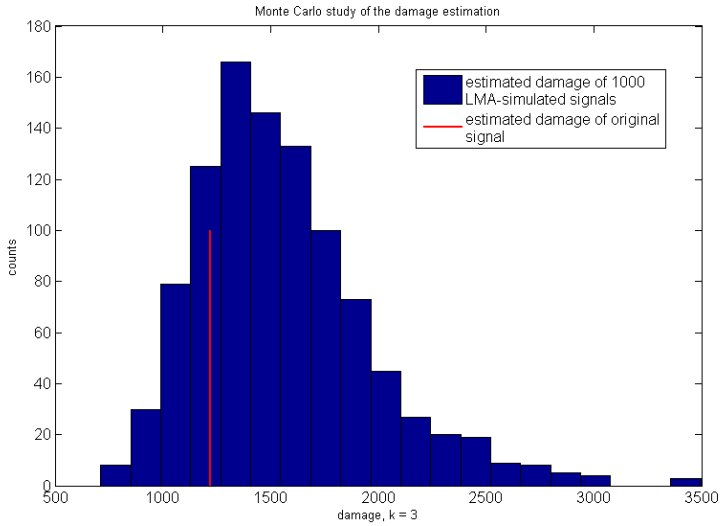


Figure 18: Histogram of estimated damage in Monte Carolo study. Notice that the estimated damage of the simulated signals slightly overestimates the damage of the original signal.

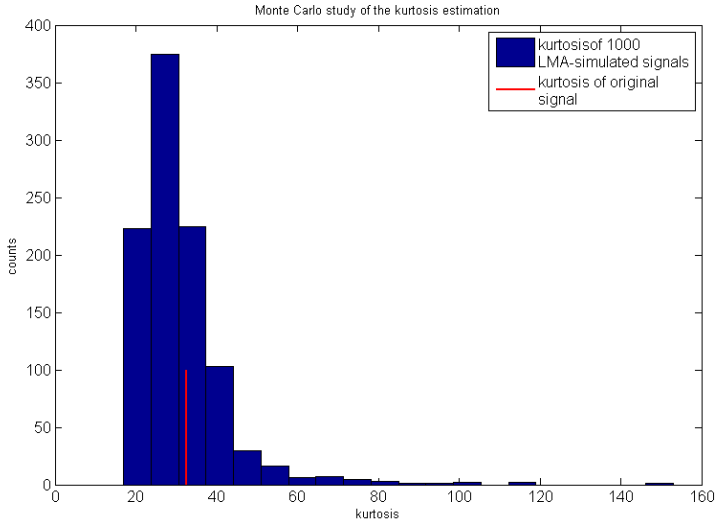


Figure 19: Histogram of estimated kurtosis in Monte Carolo study

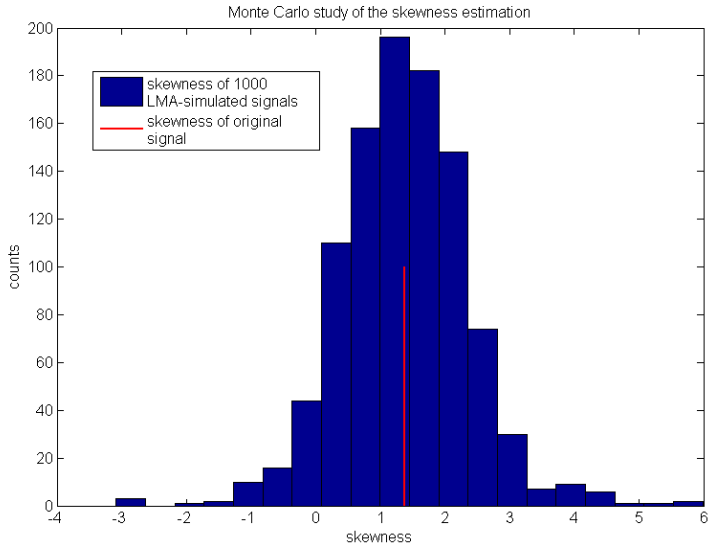


Figure 20: Histogram of estimated skewness in Monte Carolo study

## 5.2 Monte Carlo study of the empirical possibility of damage overestimation

The damage value of simulated load signals being slightly overestimated has important consequences for the success of machine design. On one hand the simulation method will give conservative fatigue life prediction which adds safety, on the other hand it makes economic design possible since designers don't need to waste unnecessary materials to guarantee the life expectation. But existence of damage overestimation in simulation from one original loaded data is not sufficient to justify the general tendency of damage overestimation. Therefore we need to apply the Monte Carlo study to the rest of 59 loaded signal processes to find out the empirical probability of damage overestimation. This investigation takes two steps:

1. For each signal process, do the 3 steps in Section 5.1. Now we have $60 \times 1000$ damage values.

2. Calculate the percentage of the event damage overestimation, i.e.,
   damage values of simulated signals $\geq$ damage value of the original signal in each group of 1000 simulated signals with respect to 60 loaded signals. As a result, one obtains a $60 \times 1$ vector with the percentage value in each component.

Figure 21 gives the histogram of the 60 percentage values with the mean percentage shown in red. We can see that on average, around 80% of the damage estimation of the LMA simulated signals is beyond the damage of the original data.

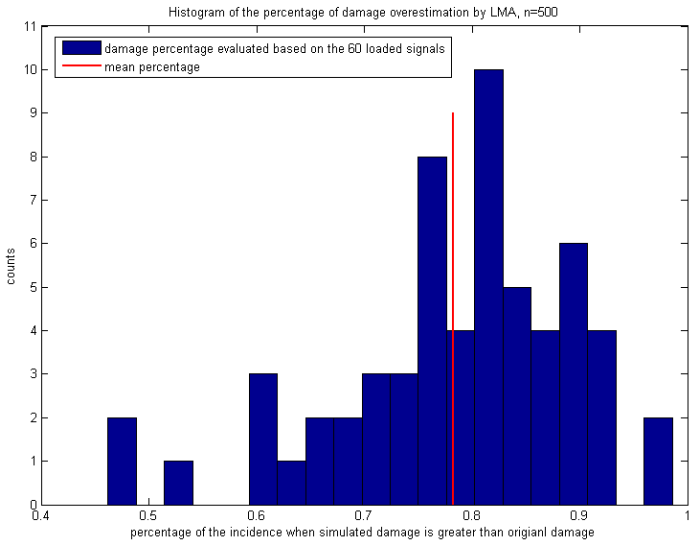


Figure 21: Histogram of the percentage of simulated damage values greater than the sample damage evaluated over 60 data files. The empirical probability of damage overestimation by LMA is around 80%.

But we notice that there are a few times for which the damage has less than 60% probability of overestimation . It is interesting to check if a low damage value of the data is related to a reduced chance of damage overestimation. If this is the case, then we won't need to worry about this occasional low percentage during machine desgin as small damage is less critical in causing machine fatigue. Lack of damage overestimation will not bring down the reliability of the design too much. To investigate this question, we plot the damamge against the corresponding percentage of damage overestimation and the result is shown in Figure 22.

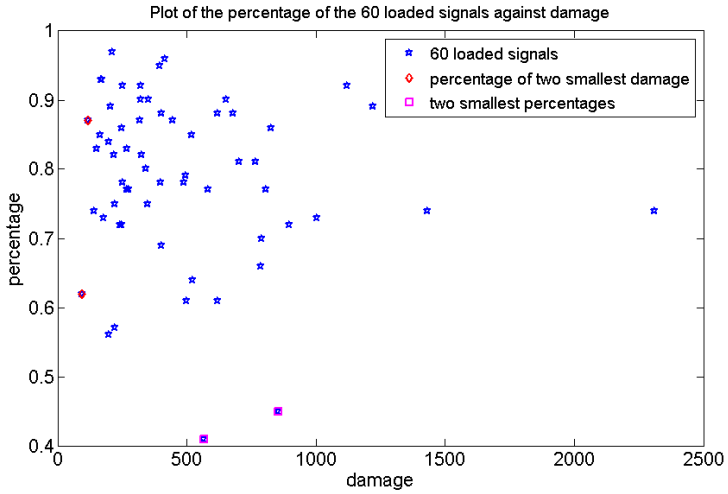


Figure 22: Plot of the percentage corresponding to damage of the 60 loaded signals. The two dots that correspond to the smallest damage value are drawn as red diamonds and the two dots with the two smallest percentage of damage overestimation are indicated by square in magenta. We notice that small damage does not incur small possibility of overestimation of damage. So one might encounter around 50% chance of damage underestimation by LMA simulation even though the damage of the signal itself is large.

Observing above figure, however, we see that there is no evidence to justify the correspondence of small damage with small possibility of damage overestimation. The two points with less than 50% possibility of damamge overestimation are highlighted by red $\Diamond$ symbol and the two points supported by the two smallest damage values are displyed by magenta $\square$ symbol. The two smallest damage values are: 96.63 and 119.87. However the damage values corresponding to the two smallest percentages are 564.87 and 852.98. We notice that they lay apart evidently. So it is not safe to completely rely on the damamge overestimation in LMA as sometines simulated loads underestimate material damages which are actually quite high.

# 6 Variability study

## 6.1 Variability analysis over single loaded signal

In real applications, we want the simulation process to be as efficient as possible without compromising too much with the result accuracy. So another interesting question we want to know is how well a single simulated LMA signal can represent the 60 loaded signals in the sense of parameter recapturization. If each group of simulated LMAs represents well the characters of the all the original data, we say that the data has small variability. Therefore we can save our effort in the future simulation as we can simply rely on one time of simulation and take it as a good representation of all the signals. Variability analysis is exceptionally interesting when data samples are coming from populations with different characters since it describes the difference of output characters within each experiment as opposed to between experiments. It consists of following two steps:

1. Apply Monte Carlo study on one original load signal as described in Section 5.1.
2. Compute the related sample characteristics from the 60 data files and those from the simulated group of signals.

The results of variability are presented in boxplots. In the boxplot, the media is symbolized by the red line. The upper and lower surface of the box cover the first and the third quartile of the data. The top black bar corresponds to the lowest value which is larger than [the first quartile $- 1.5 *$ (the third quartile $-$ the first quartile)]. The lower black bar represents the highest value which is smaller than [the third quartile $+ 1.5 *$ (third quartile $-$ first quartile)]. Outliers are marked by red crosses. We apply Monte Carlo simulation to data of tine 3 section 1 and 2 in `CS80-10-10-10-02`. In Figure 23 we see that the estimated damage from a single simulated group is unable to cover the damage values of all the loaded signals. The blue dotted line is the parameter of the signal we used to generate the group of simulated signals. The same phenomenon shows up in the variability analysis of skewness and kurtosis shown in Figure 24 and 25.

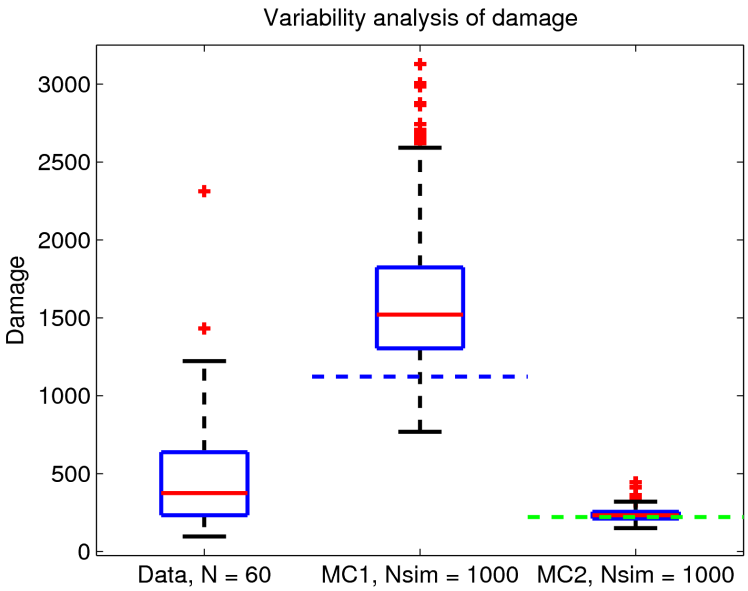


Figure 23: Boxplot of the damage estimation of 60 loaded signals and of 1000 LMA simulated signals. Left: boxplot of estimated damage obtained by 60 original loaded data. Middle: boxplot of estimated damage calculated from 1000 simulated LMA signals generated from data set tine 3 section 1 in `CS80-10-10-10-02`. Right: boxplot of estimated damage calculated from 1000 simulated LMA signals generated from data set tine 3 section 2 in `CS80-10-10-10-02`. We can see that it is not possible to capture the entire variability of damage by a single signal.

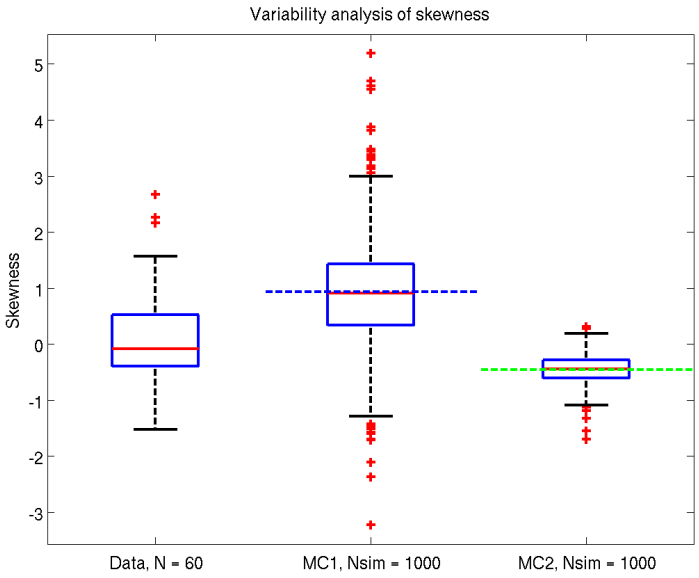


Figure 24: Boxplot of the skewness of 60 loaded signals and of 1000 LMA simulated signals. Left: boxplot of skewness of the 60 original loaded data. Middle: boxplot of skewness of 1000 simulated LMA signals generated from data set tine 3 section 1 in `CS80-10-10-10-02`. Right: boxplot of skewness of 1000 simulated LMA signals generated from data set tine 3 section 2 in `CS80-10-10-10-02`. We can see that it is not possible to capture the entire variability of skewness by a parameter set calculated based on single signal.

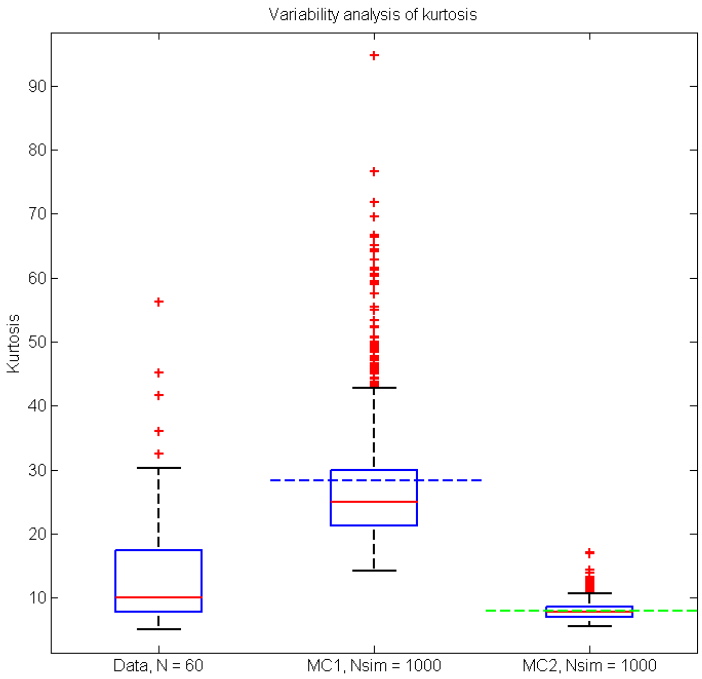


Figure 25: Boxplot of the kurtosis of 60 loaded signals and of 1000 LMA simulated signals. Left: boxplot of kurtosis of the 60 original loaded data. Middle: boxplot of kurtosis of 1000 simulated LMA signals generated from data set tine 3 section 1 in `CS80-10-10-10-02`. Right: boxplot of the kurtosis of 1000 simulated LMA signals generated from data set tine 3 section 2 in `CS80-10-10-10-02`. We can see that it is not possible to capture the entire variability of kurtosis by a parameter set calculated based on single signal.

## 6.2 Variability analysis by bootstrap with non-parametric model

The above analysis shows that a simulated load signal from single data set cannot include the parametric characteristics of the 60 loaded signals. One possible way to increase the variability of the output characteristic of a sample of simulated signals is to randomize the parameters that are used to generate each simulated signal. This can be done, for example, by bootstrapping from the 60 parameter sets that we have observed or by parameterization of the underlying parameter set. The rest of analysis are based on these two kinds of study. Bootstrapping with a non-parametric model includes the following two steps:

1. Randomly draw a sample from the 60 loaded signals. Generate one LMA-simulated signal by parameters of the selected sample and calculate the sample characteristics

of this simulated signal.

2. Repeat previous step for N times to obtain a pool of parameter sets with length N.

In the following boxplot, we compare the scatter of the output characteristics of the 60 loaded signals and the one of the 1000 simulated signals which is generated by parameters obtained by bootstrapping from the parameter sets of the 60 original data. We notice that in Figure 26 of damage comparison, the values within the whisker bars agree but simulated signals produce very high outliers. The agreement is more obvious in the kurtosis boxplot in Figure 27. Furthermore, the median values of damage of the simulated signals are almost the same as in the original loads.

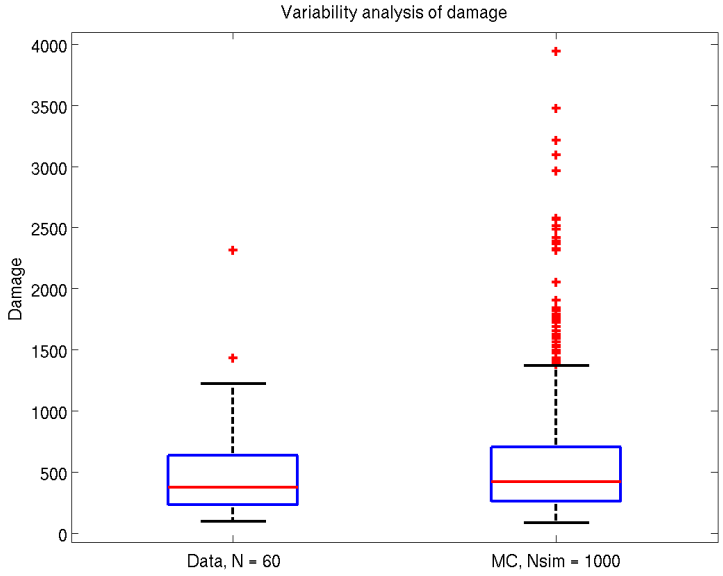


Figure 26: Boxplot of the damage estimation of 60 loaded signals and of 1000 LMA simulated signals generated by bootstrap. Left: boxplot of estimated damage obtained from 60 original loaded data. Right: boxplot of estimated damage of 1000 simulated LMA signals with each based on bootstrapped parameters from the 60 parameter sets. We can see that within the whisker bars, the simulated signal covers the damage character of the original data very well. But it also generates heavy outliers.

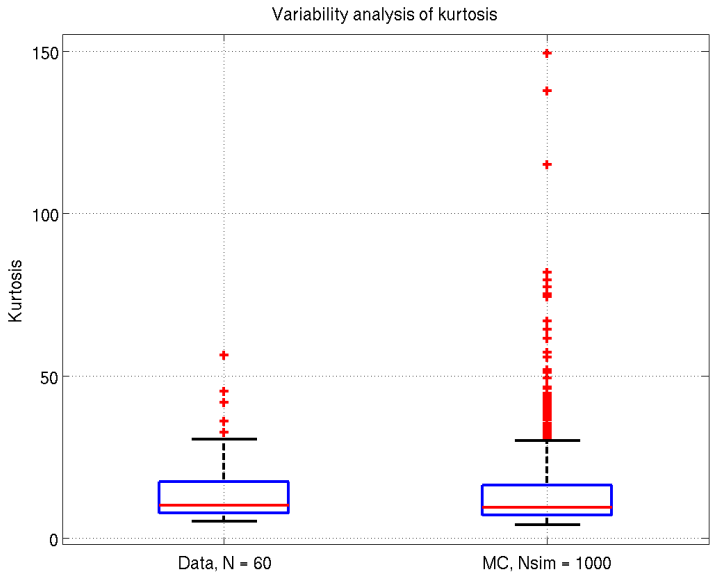


Figure 27: Boxplot of the kurtosis estimation of 60 loaded signals and of 1000 LMA simulated signals generated by bootstrap. Left: boxplot of kurtosis of 60 original loaded data. Right: boxplot of kurtosis of 1000 simulated LMA signals with each based on bootstrapped parameters from the 60 parameter sets. We can see that within the whisker bars, the simulated signal has almost the same damage character as the original data's. But it also contains heavy outliers.

## 6.3 Variability analysis by bootstrap with parametric model

Another method of variability analysis is to bootstrap from a parametric model that is fitted to a parameter set. Since we have noticed that the kurtosis of a signal process has the biggest impact on the accuracy of damage approximation, now we will focus on the distribution fitting to the 60 kurtosis values obtained from original loaded data. We fix the spectral density as the mean value of the 60 sample spectral densities. Therefore the kernel function is fixed in this case. Since the average skewness is mildly different from zero and it is less decisive for damage estimation, for the sake of simplicity we consider it as a constant equal to zero. After some exploration, we find out Gamma distribution gives the best approximation of the histogram of the kurtosis among other alternatives. Four out of the sixty kurtosis values deviate from the major values so we remove them for better parameter estimation. The two parameters of the Gamma distribution are estimated by the maximum likelihood method. Figure 28 shows the density function of the fitted Gamma distribution together with the histogram of the kurtosis values. We notice that the shape of the density function captures the characteristics of the empirical distribution of the kurtosis, but the fitness is not promising. We have low

fitted density for low kurtosis values. Therefore kurtosis from the Gamma distribution can have a great chance to generate high kurtosis that leads to extremely big damage. This corresponds to the outrageous outliers in Figure 30. We also notice that the fitted Gamma density in the upper region is very low and major kurtosis is gathered around 5 to 8. But nevertheless the LMA simulated signals produce high damages. This might be related to the damage overestimation of the LMA simulation algorithm. In Figure 29, we plot the kurtosis against the percentage of damage overestimation as we did in Section 5.2. According to this figure, high kurtosis does not indicate high chance of damage overestimation. However kurtosis with high density lying between 5 and 8 in Figure 28 has more than 70% chance to generate overestimated damage. So without high kurtosis values, LMA simulation can still reproduce high damage.

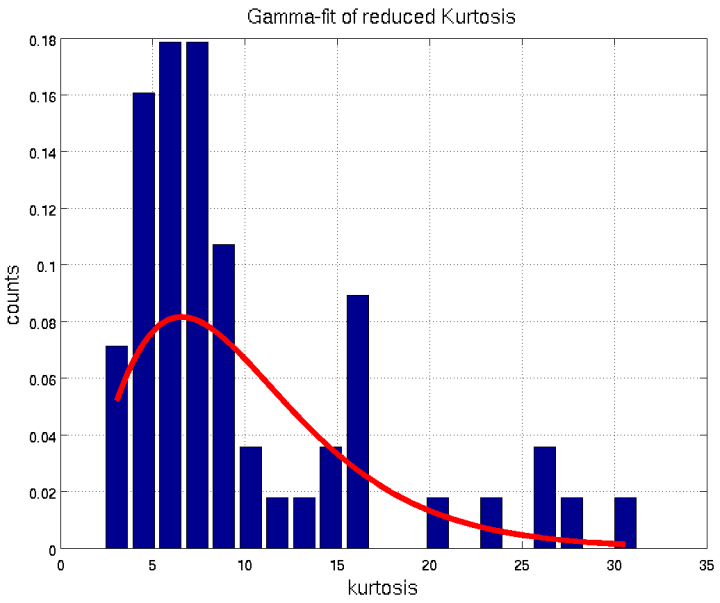


Figure 28: Fitted-Gamma distribution to the 56 kurtosis values.

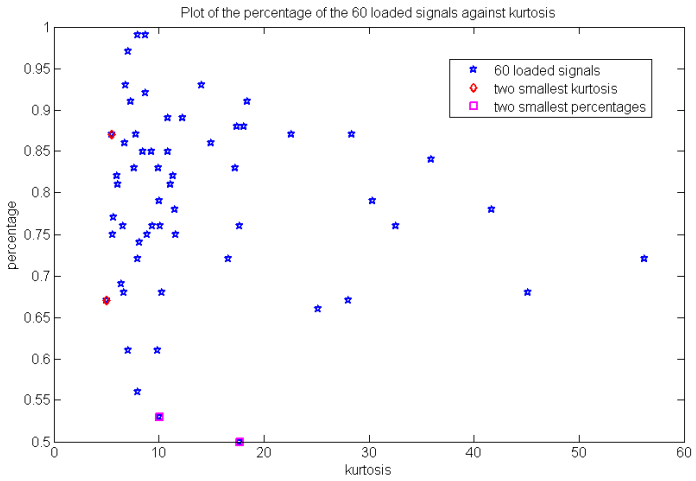


Figure 29: Plot of the percentage corresponding to kurtosis of the 60 loaded signals. The two dots of percentage corresponding to two smallest kurtosis are drawn as asterisks in red and the two dots with the two smallest percentages of damage overestimation are indicated by squares in magenta. We notice that small kurtosis does not incur small possibility of overestimation of damage. However, in the region of high density of kurtosis, the possibility of damage overestimation clusters around 0.7 to 0.95. This indicates that most kurtosis will result in high damage estimation due to high possibility of overestimation.

In the following two figures, we bootstrap 1000 values from the Gamma distribution and use them to generate LMA-simulated signals. For demonstration, we now only look at the variability of damage values. In Figure 30, both boxplots of damage are calculated from standardized signals, i.e, signals which have been divided by their standard deviation after subtracting the mean so that the standardized signals have zero mean and standard deviation one. We notice that the variability is sufficient to cover the spread of the original data. But compared to the damage distribution from the non-parametric bootstrap in Figure 26, the outliers seem to be less extreme. This might relate to the removal of the 4 outstanding kurtosis values during the model fitting of kurtosis. As a result, the parametric bootstrap method will generate less excessive kurtosis and therefore produce a more conservative damage estimation. So one may not compare the right hand side of Figure 26 to the one of Figure 30 as the analyses are not built on the same ground.

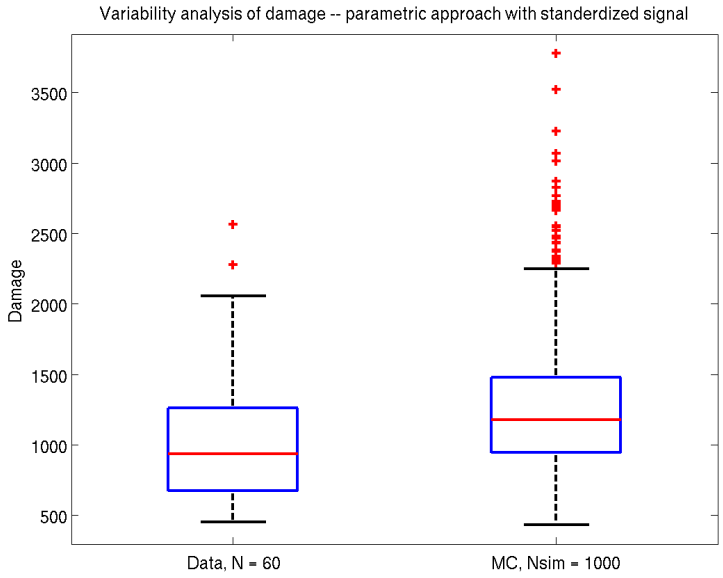


Figure 30: Boxplot of the standardized damage estimation of 60 loaded signals and of 1000 LMA simulated signals generated with kurtosis bootstrapped from a Gamma distribution. Left: boxplot of the damage estimation of the 60 loaded signals. Right: boxplot of the damage estimation of the 1000 LMA simulated signals. Notice that the simulated signals still contain heavy outliers. Different from the non-parametric study in Figure26, the median lies above the one of the original.

Compared with the parametric bootstrap, the non-parametric bootstrap seems to be a more desirable way to extend variability. Both of them have sufficient variability to capture the full sample characteristic of the 60 data sets. But due to the lack of fitness of the sample kurtosis to the Gamma distribution, the parametric bootstrap produce increased distribution of sample characteristics such as damage. The low numbers of 60 data units is too little to obtain a suitable parametric model. Therefore nonparametric bootstrap serves as a better way to increase variability without deviating too far from the true performance of the original data. In general at the current stage of study, we have too little data in to conduct a thorough examination of the variability. When we have data from different fields or loading conditions, we can do a more extensive study of variability of the sample characteristics.

# 7 Multivariate signal modeling

## 7.1 Correlation analysis of one channel

So far we have only looked at the loads of force in the Y direction, that is, Fy in the data. Signals from channels like forces in X and Z direction, i.e., Fx, Fz and the momentum values in these three directions Mx, My and Mz are left unstudied. However, since the cultivator prototype has a stiff structure, every stress is a linear combination of individual signals. So they are highly linearly correlated in the damage creation. Furthermore, it is interesting for us to find out the maximal damage among all linear combinations of loads. The most straightforward way to study the linear correlation between random variables is by their covariance matrix or the correlation matrix. Once the covariance matrix is obtained, one can use the principal component analysis (PCA) to look for the eigenvector corresponding to the largest eigenvalue so that we can construct a combined virtual signal which has greatest variance among all the original data. If variance is a significant element in fatigue damage creation, the combined signal can be used as a bounding signal in the perspective of damage estimation. Of course if variance is not as decisive as other alternative elements, the combined signal will not induce damage values higher than its components. So PCA can also help us to evaluate the importance of variance in damage prediction. From now on, we only focus on data with all three tines loaded, that is, only data from the file `CS80-10-10-10`. First of all, we look at the covariance matrix obtained from data Fy of repetition 2 section 3. Its covariance is given by the $3 \times 3$ matrix

$$\text{covariance} = \begin{pmatrix} 0.6492 & -0.1371 & 0.0863 \\ -0.1371 & 0.8138 & -0.0998 \\ 0.0863 & -0.0998 & 0.7071 \end{pmatrix}. \tag{7.1}$$

The corresponding correlation matrix is

$$\text{correlation} = \begin{pmatrix} 1.0000 & -0.1886 & 0.1274 \\ -0.1886 & 1.0000 & -0.1316 \\ 0.1274 & -0.1316 & 1.0000 \end{pmatrix}. \tag{7.2}$$

We notice that the correlations between two tines are not very significant. Also negative correlations between two adjacent tines are evident in the correlation matrix. This is a natural consequence of the linear structure.

Now, we present the basic steps of principal component analysis. The procedure is carried out by the covariance method of the principal component analysis (PCA). It involves the following four steps:

1. Choose the group of data one wants to analyze. In our case, the data matrix has its column number as the number of channels we include in our analysis and the row number as the length of each signal. We denote the data by $X = \begin{bmatrix} x_1 & x_2 & x_3 \end{bmatrix}$.

2. Calculate the covariance matrix $cov(X)$ of the data matrix $X$.

3. Apply singular value decomposition on $cov(X)$, that is, decompose $X$ into $X = U * S * V^T$. Here $U$ and $V$ are two unitary matrices and $S$ is a diagonal matrix with its entries sorted in a decreasing order. $T$ represents transpose. Find out the main influential components by taking the biggest singular values in $S$. The corresponding column vector in the unitary matrix $U$ is denoted by $a$.

4. Multiply $a$ with the data matrix $X$ to obtain the reduced signal set.

Applying PCA to these three signals, we obtain as the first column of the unitary matrix: $a = \begin{bmatrix} -0.4640 & 0.7571 & -0.4598 \end{bmatrix}^T$. The combined signal is constructed by $-0.464 * x_1 + 0.7571 * x_2 - 0.4598 * x_3$ where $x_1$, $x_2$ and $x_3$ represent three signals. The individual signals and the combined signal are shown in Figure 31.

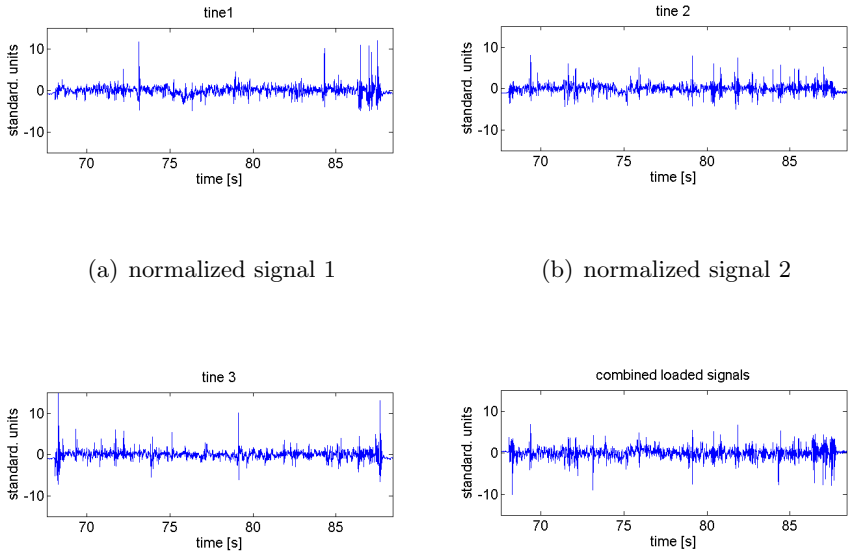


(a) normalized signal 1

(b) normalized signal 2

(c) normalized signal 3

(d) combined signal

Figure 31: Individual normalized signals and their combination

The sample characteristics of the individual tines and the combined signal are given in Table 4.

Table 4: Moments and damage characteristics of the three individual signals and the combined signal. The combined signal has greatest variance. But its damage is smaller than the one of tine 3. Noticing that tine 3 has significantly high kurtosis, one should understand that kurtosis has higher influence to damage estimation than variance.

| | std. deviation | skewness | kurtosis | damage |
|---|---|---|---|---|
| tine 1 | 0.8 | 1.1 | 18.1 | 768.3 |
| tine 2 | 0.9 | 0.6 | 8.5 | 681.6 |
| tine 3 | 0.8 | 1.4 | 32.6 | 1222.2 |
| combined | 1 | 0.1 | 8 | 1118.1 |

From Table 4, we see that although the combined signal has the greatest variance, it's damage expectation value 1118.1 is still smaller than the damage of the single tine 3 1222.2. During the analysis in previous sections, we have recognized the importance of high kurtosis in damage creation. As a result, the exceptionally high kurtosis of tine 3 is the main reason for the high damage. The combined signal only has kurtosis equal to 8, being only one forth of the kurtosis of the tine 3, therefore it does not have as many or as high extreme values as tine 3, hence the damage value is lower. To further confirm this phenomenon, we evaluate the damage of an individual signal and the combined signal of all the 6 data sets coming from the 2 times of repetition and 3 sections. The findings are given in Table 5.

Table 5: Estimated damage of the three individual signals and the combined signal of all the 6 sections. The highest damage value is highlighted in boldface. Obviously the variance maximized signal does not promise damage maximization. In 5 out of 6 experiments, the combined signal has lower damage characteristics than a single signal's.

| | Tine 1 | Tine 2 | Tine 3 | Combined |
|---|---|---|---|---|
| Data 1 | **521.6** | 169.4 | 350 | 486 |
| Data 2 | **786.6** | 213.9 | 564.9 | 549.9 |
| Data 3 | 620.5 | 415.8 | **2312.5** | 1905.4 |
| Data 4 | 248.1 | 324.8 | **1122** | 720.7 |
| Data 5 | 222.5 | 619.8 | 221.7 | **691** |
| Data 6 | 768.3 | 681.6 | **1222.2** | 1118.1 |

We notice that in Table 5, only in data 5, the combined signal possesses highest damage. In most cases, the damage value corresponding to the combined signal is smaller than the value of a marginal signal. So by maximizing over variance, we cannot obtain a signal that bounds other signals in the sense of damage creation. Variance is a undeniably important element in fatigue analysis. But compared to a homogeneous load

signal with constant and big amplitudes, loads having irregular huge extreme values are more susceptible to the damage since material fractures easily happen when stress has drastic changes.

Another way to explain the insignificance of the damage of the combined signal is based on the properties of PCA. As we can notice from the correlation matrix of the three signals in (7.2), the correlations between each pair of two tines are negligible – the values are around 0.1. The weak correlations reduce the power of PCA to produce a combined signal with variance of a large increase so it fails to give useful results.

## 7.2 Correlation analysis of the 18 channels

For the sake of simplicity, in this section, we only look at the loaded situation of repetition 1 section 2. Each of the three loaded tines has 6 measurements to describe its momentum and force in $X$, $Y$ and $Z$ directions. So in total we have $3 \times 6 = 18$ signals. We display the correlation matrix of these 18 signal vectors by the 'imshow' in figure 32. The imshow function in MATLAB reflects the significance of the correlation by image grayscale. The highest correlation, which is 1 is displayed as white. The lowest correlation is displayed as black. Values between 0 and 1 are shown as intermediate shades of gray. The brighter the pixel looks, the higher the correlation value is. In figure 32 we see very obvious strong correlations exist between some pairs of signals.

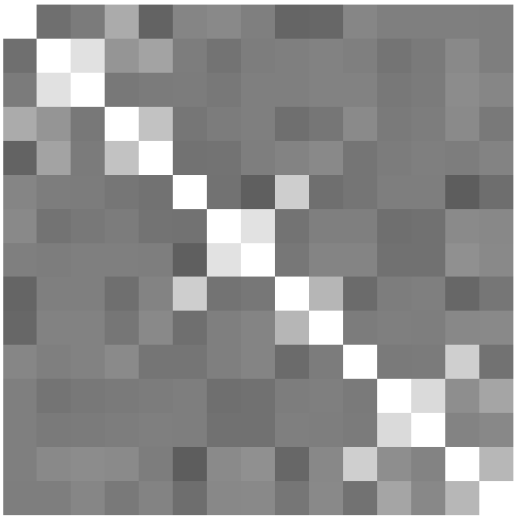

Figure 32: Imshow of the correlation matrix of the 18 signals

Now we apply PCA to the 18 signal vectors. Parameters of marginal signals and the combined one are given in the following table. We notice that this time the combined signal does produce the greatest damage, furthermore the kurtosis is no longer very

small. Although here PCA seem to work and produces the expected result, we might be risking doing senseless test due to lack of knowledge of the damage accumulation mechanism with so many various physical measurements. How does momentum influence the rainflow damage estimation? How much damage did we calculate repeatedly by including different related measurements? To find out answers to these questions, or to truly obtain a reasonable damage-maximized signal, we need further study of signal modeling of the correlation between different tines. Some alternative methods are proposed in the next section.

Table 6: Parameters of the 18 signals and the combined signal. We notice that the damage value of the combined signal is higher than any of the 18 marginal signals. Different from the combined signal in Table 4, the kurtosis of the combined signal based on the 18 channels has reasonably big kurtosis.

| no. | std. deviation | skewness | kurtosis | damage |
|---|---|---|---|---|
| 1 | 0.4 | 2.7 | 19.8 | 68.9 |
| 2 | 0.3 | 0.5 | 6.3 | 10.6 |
| 3 | 0.2 | 0.6 | 7.3 | 1.1 |
| 4 | 0.3 | 0.3 | 6.8 | 37.1 |
| 5 | 0.8 | 0.5 | 10.8 | 647.2 |
| 6 | 1.2 | -1.4 | 18 | 2802.4 |
| 7 | 0.6 | 3.2 | 36.9 | 200.4 |
| 8 | 0.2 | 0.5 | 6.8 | 6.8 |
| 9 | 0.2 | 0.7 | 6 | 3.0 |
| 10 | 0.3 | 0.8 | 14.1 | 26.9 |
| 11 | 0.9 | -0.8 | 8.2 | 452.6 |
| 12 | 0.8 | -1.3 | 7.8 | 247.8 |
| 13 | 0.6 | 6.2 | 79.4 | 268.5 |
| 14 | 0.3 | -0.2 | 6.7 | 11.9 |
| 15 | 0.1 | 0.3 | 4.6 | 0.7 |
| 16 | 0.4 | -0.2 | 7.3 | 51.3 |
| 17 | 0.9 | 2.4 | 51.9 | 1999.2 |
| 18 | 1.2 | 1.9 | 28.2 | 3089.1 |
| Comb | 1.3 | -0.1 | 21.5 | 4491.2 |

# 8 Conclusion and discussion

This report shows that the Laplace moving average process is a successful model for loads on marginal tines which have high third and forth moments. It gives slightly over-estimated damage computed by rainflow cycle counts which makes it very useful in machine design as it balances very well between conservativeness and economy. As shown by the Monte Carlo study with all loaded data, almost 80% of the damage of the LMA simulated signals is overestimated. But in some situations big damage may have around 50% chance to be underestimated so solely relying on the model carries a certain risk. Kurtosis is the most critical element for better damage approximation as we recognize the high peaks in the load cause major damage computed by rainflow cycle counts.

In order to investigate the difference of output characteristics within each experiment as opposed to between experiments, we applied variability analysis to the 60 loaded signals. The result shows that statistics such as damage, kurtosis and skewness captured by a single signal cannot represent the range of statistics of different load signals. Randomizing the parameter set used to generate LMA signal by bootstrap can increase variability and we carried out such a study in two ways: the non-parametric bootstrap and the parametric bootstrap. In the non-parametric bootstrap, parameter sets are drawn with equal probability from the parameter pool of the 60 load signals and they are used to simulate 1000 LMA signals whose characteristics such as damage and kurtosis are compared to the original data's. Both the damage and kurtosis of the LMAs that are generated by means of non-parametric bootstrap cover the range of corresponding characteristics of the original data very well. But the outliers scatter vastly above the top whisker bar in the boxplot. In the parametric bootstrap, we focused on the distribution of kurtosis and fitted a Gamma distribution to the 60 kurtosis values obtained from loaded data. By fixing the spectral density at its mean value and the skewness at zero, we generated 1000 LMAs whose kurtosis are drawn randomly from the fitted Gamma distribution. In this case, the variability of estimated damage of LMAs is also capable to cover the range of the damage of all the original loaded signals. But heavy outliers are still observed in the boxplot. Since 60 values of kurtosis are too little to obtain a good fit of the parametric model, the variability presented by parametric bootstrap is less reliable than the non-parametric one, although the differences in the outputs are not very obvious. After all, variabilities among different experiments will become more worthwhile to study after we have obtained more verified data such as from different fields or from different driving patterns.

In multivariate signal analysis, we give our attention to the linear structure of the system and are interested in finding a combined signal that causes greatest damages among all loaded signals. We call such a signal a damage-bounding signal. Since searching for the damage-maximized signal in all possible directions is not readily accessible, principal component analysis(PCA) is used to produce a variance-maximized signal, which is the linear combination of all marginal signals under consideration. But PCA fails to generate a damage-maximized signal as we observed in the correlation analysis

of channel Fy when all three tines are loaded, the variance-maximized combined signal is not the damage-maximized signal. This is due to the weak capture of the kurtosis in the variance-maximized combined signal. However on the other hand, if we apply PCA over 18 channels which respectively describe different physical measurements of loaded tines, it seems by this way we can correct the weak point in the previous analysis as the variance-maximized signal not only presents the highest damage but also a high value of kurtosis. But since we have not explored the reasonability of such an analysis, we did not justify whether including momentum in rainflow damage estimation is reasonable or not. It is possible that including too many related measurements will repeatedly calculate damage. So further study of the relationship between force and momentum in all three directions is needed to explain their collaborative influence to the rainflow damage.

The results of PCA in multivariate signal modeling suggest that in order to produce a damage-bounding signal, maximization over variance is not sufficient, although it is true that if a signal has high kurtosis, its variance will also preserve high value since frequent extremes will increase the average deviation from the mean. So looking over the variance-maximized signal is a natural first step to seek for a damage-maximized signal. But the result justifies that kurtosis is of greater importance than any other elements in looking for the direction of damage maximization. In the next step of signal search, we should include kurtosis maximization. This can be realized by applying PCA over the covariance matrix of signals $Y_i = \text{sign}(X_i)X_i^2$ to find the direction with highest kurtosis.

Another possible way to improve the direction search is to maximize the damage function over all possible coefficients involved in the construction of the linear-combined signal. That is, if $a$ is a column vector of coefficients with norm 1 and X is the data set with each of its columns being a signal, we want to look for the vector $a_{max}$ satisfying

$$a_{max} := \text{argmax}(\text{Damage}(Xa)) \text{ under the constraint } \textstyle\sum_i a_i^2 = 1$$

where $a_i$s are components of vector $a$. That is, we maximize the damage over the whole sphere of possible values of $a$. Then based on the 6 parameter sets corresponding to occasions when all three tines are loaded, for every group of three simulated LMA signals representing three simultaneously loaded signals, we can search for the direction that gives the maximum damage. Then we can calculate the damage corresponding to the mean direction or the average of maximum damage generated by individual groups of LMAs. The distribution of the maximum damages is also interesting to investigate.

Another phenomenon we want to look into more closely is the modeling of the correlation between different tines. One fundamental property of the stiff structure is the linear combination of the signals in the stress creation. Therefore it is natural to expect high correlation between loaded tines. However as we noticed in Section 7.1, when all the three tines are loaded, against our expectation, the correlations between these tines are not very strong. It is not known if this is due to the resonance canceling out the dynamics or the measurement of the vibration not being refined enough to reveal the correlation. Another possible explanation is that the transmission dynamics of the structure — force in Y direction between tines simply have no clear correlations. So

further studies are required to fully explain the physical properties of the dynamics in the structure.

Last but not least, follow-up study of the spectral density is required for an extended variability analysis. In this paper, we only consider a symmetric kernel. This is based on the assumption that driving in one direction and in its opposite won't change the spectrum of the signal. But in practical procedures, once the tine is at work, it might keep being loaded even during turning, so an asymmetric kernel might be used to simulate the turning condition. Since the kernel function is directly related to the spectral density in simulation, modeling of the spectral density will be a decisive task in capturing the variabilities such as soil condition or driving habit.

# Appendices

## A Spectral moments and Rice formula

The same as stated in section 4, the underlying random process $Z(t)$ is assumed to be a zero mean process. The following theorems presents some very important properties of a stationary process, especially a Gaussian process. Proofs of these theorems under more general conditions can be found in [5]. We first give the definition of a stationary process:

**Definition 7** (Stationary process in the strict sense)**.** *The process is called stationary if for any $\tau$ the vectors $Z(t_1), Z(t_2), \cdots, Z(t_n)$ and $Z(t_1+\tau), Z(t_2+\tau), \cdots, Z(t_n+\tau)$ have the same distribution.*

Definition 5 in section 4 tells that the autocorrelation $R_z(\tau)$ of a random process $Z(t)$ is the inverse Fourier transform of the spectral density $S_z(\omega)$, i.e.,

$$R_z(\tau) \Longleftrightarrow S_z(\omega).$$

stating that the autocorrelation function is the Fourier transform pair of the spectral density. It is natural to see that when $\tau = 0$, we have such equality that

$$R_z(0) = \mathrm{Var}[Z(t)] = \int S_z(\omega) d\omega := \lambda_0. \tag{A.1}$$

Moreover, according to the time differentiation law of Fourier transform operations, we have Fourier pair of the second order derivative of the autocorrelation function:

$$R_z^{''}(\tau) \Longleftrightarrow (i\omega)^2 S_z(\omega).$$

where $i$ is the imaginary unit. Therefore we have

$$-R_z^{''}(\tau) = \int e^{i\tau\omega} \omega^2 S_z d\omega. \tag{A.2}$$

Also by applying derivative over $\tau$ on both sides of (4.3) and exchanging the order of differentiation and integration operation, we have

$$\frac{dR_z(\tau)}{d\tau} = \mathrm{E}\left[Z(t)\dot{Z}(t+\tau)\right]. \tag{A.3}$$

where $\dot{Z}(t+\tau)$ indicates the derivative process of $Z(t+\tau)$. Since the ensemble average of a stationary process is independent of the time, we have

$$\frac{dR_z(\tau)}{d\tau} = \mathrm{E}\left[Z(t)\dot{Z}(t+\tau)\right] \tag{A.4}$$

$$= \mathrm{E}\left[Z(t-\tau)\dot{Z}(t)\right]. \tag{A.5}$$

Differentiating over $\tau$ on both sides of (A.4), we have

$$\frac{d^2R_z(\tau)}{d^2\tau} = -\,\mathrm{E}\left[\dot{Z}(t-\tau)\dot{Z}(t)\right]. \tag{A.6}$$

where $\dot{Z}(t-\tau)$ is the derivative process of $Z(t-\tau)$ and $\dot{Z}(t)$ is the derivative process of $Z(t)$. If $\tau = 0$, (A.6) shows that

$$-R_z^{''}(0) = \mathrm{Var}[\dot{Z}(t)] \tag{A.7}$$

indicating that the variance of the derivative process of $Z(t)$ is equal to the second order derivative of the autocorrelation function while evaluated at 0. Plug the RHS of (A.2) with $\tau = 0$ into previous equality, we have

$$\mathrm{Var}[\dot{Z}(t)] = \int \omega^2 S_z d\omega :\equiv \lambda_2. \tag{A.8}$$

(A.1) and (A.8)represent the form we call spectral moments and it is defined as

$$\lambda_i = \int \omega^i S(\omega) d\omega \tag{A.9}$$

where $\lambda_i$ is the $i$th spectral moment. Spectral moments have very important meaning in stochastic signal processing as it connects the variance of a stochastic process and its derivative processes to the spectral density function which is very easy to compute numerically.

Another important property of a stationary process is given by following theorem.[11]

**Theorem 8.** *A stationary process the derivative $\dot{Z}(t)$ is uncorrelated of $Z(t)$. i.e., $E(Z(t)\dot{Z}(t)) = 0$.*

*Proof.* First we introduce an operation $e^{aD}$ where $D$ indicates differentiation operation. By treating $D$ as a number and then using the Maclaurin series, we obtain:

$$e^{aD} = \sum_{k=0}^{\infty} \frac{a^k D^k}{k!}$$

where $D^k$ means the k-th order derivative. Applying such an operation over a function $f(x)$, we get

$$e^{aD} f(x) = \sum_{k=0}^{\infty} \frac{a^k}{k!} f^{(k)}(x) = f(x+a). \tag{A.10}$$

We define the operation of $e^{aD}$ by (A.10). Substituting $f(x)$ by $Z(t)$ which is a stationary process and $a$ by $\tau$ to indicate the time increment, we get

$$e^{\tau D} Z(t) = Z(t+\tau) \tag{A.11}$$

Differentiate over $\tau$ in (A.11) on both sides, then

$$e^{\tau D} DZ(t) = \frac{dZ(t+\tau)}{d\tau}. \tag{A.12}$$

By letting $\tau = 0$ to compute the derivative at 0 on the right hand side of (A.12), we obtain

$$\frac{dZ(t+\tau)}{d\tau}|_{\tau=0} = DZ(t) = \frac{dZ(t)}{dt}. \tag{A.13}$$

Similarly, we can show that

$$\frac{dZ(t-\tau)}{d\tau}|_{\tau=0} = -DZ(t) = -\frac{dZ(t)}{dt}. \tag{A.14}$$

Knowing from the symmetry of autocorrelation, we have $E(Z(t)Z(t+\tau)) = E(Z(t)Z(t-\tau))$. Since the autocorrelation exits, we can differentiate it over $\tau$ and obtain

$$E[Z(t)\frac{dZ(t+\tau)}{d\tau}] = E[\frac{dZ(t-\tau)}{d\tau}Z(t)]. \tag{A.15}$$

By implementing (A.13) and (A.14) in to (A.15), we get

$$E[Z(t)\dot{Z}(t)] = -E[\dot{Z}(t)Z(t)].$$

This equality only establishes when $E[Z(t)\dot{Z}(t)] = 0$. □

Now we move on to look at the mean crossing property of a Gaussian stationary process. The final result is called Rice formula. But to begin with, we give the definition of a Gaussian process.

**Definition 9** (Gaussian process)**.** *A stochastic process $Z(t)$ is called a Gaussian process(or normal process) if any linear functional applied to the sample function $Z_t$ will give a normally distributed result.*

For a stationary Gaussian process $Z(t)$, it has the same distribution regardless what value $t$ takes. Therefore, it is easy to notice that if $Z(t)$ is a stationary Gaussian process, its samples have the same distribution regardless what value $t$ takes. So for the sake of simplicity, to use $Z(0)$ to represent a random sample of a stochastic process $Z(t)$, $t \in [0, \infty]$. Let's assume $Z(t)$ follows $N(\mu, \sigma^2)$ for all $t \in [0, \infty]$. Also since the differentiation is a linear operation, the derivative of a Gaussian process is still a Gaussian process. That is, if $Z(0)$ follows a normal distribution, its time derivative $\dot{Z}(0)$ will remain a Gaussian process.

Rice formula gives an analytical form of the expected number of zero-crossing with respect to different levels when a process is a stationary Gaussian process. Before we reach the step of proofing it, we need one last theorem about the mean crossing of a stationary process to start from.

**Theorem 10.** *For stationary loads having continuous derivative, if the joint probability density of* $(Z(t), \dot{Z}(t))$ *is known then, for almost all levels* $u$*, the expected number of crossing is*

$$\mathrm{E}[N(u)] = \int |v| f_{\dot{Z}(0),Z(0)}(v,u)dv. \tag{A.16}$$

*where* $N(u)$ *stands for the number of crossing.*

**Theorem 11** (Rice formula)**.** *If* $Z(t)$ *is a stationary normal process with finite second spectral moment* $\lambda_2 = -R_z^{''}(0)$ *then the mean number of upcrossings of any fixed level* $u$ *per unit time is finite and given by*

$$\mathrm{E}[N(u)] = \frac{1}{\pi}\sqrt{\frac{\lambda_2}{\lambda_0}} e^{-\frac{u^2}{2\lambda_0}} \tag{A.17}$$

*where* $\lambda_0$ *and* $\lambda_2$ *are defined as in* (A.9)*.*

*Proof.* As we have shown in previous discussion for a Gaussian stationary process $Z(t)$, its derivative $\dot{Z}(t)$ is uncorrelated with the process and still has the normal distribution. Since we also have known that the mean values of processes $Z(t)$ and $\dot{Z(t)}$ are both zero and variance respectively are $\lambda_0$ and $\lambda_2$, it's straightforward to derive:

$$\begin{aligned}
\mathrm{E}[N(u)] &= \int_{-\infty}^{+\infty} |v| f_{\dot{Z}(t),Z(t)}(v,u)dv \\
&= \int_{-\infty}^{+\infty} |v| \frac{1}{\sqrt{2\pi V[\dot{Z}(t)]}} e^{-\frac{v^2}{2V[\dot{Z}(t)]}} dv \frac{1}{\sqrt{2\pi V[Z(t)]}} e^{-\frac{u^2}{2V[Z(t)]}} \\
&= 2\int_{0}^{+\infty} v \frac{1}{\sqrt{2\pi V[\dot{Z}(t)]}} e^{-\frac{v^2}{2V[\dot{Z}(t)]}} dv \frac{1}{\sqrt{2\pi V[Z(t)]}} e^{-\frac{u^2}{2V[Z(t)]}} \\
&= \frac{2V[\dot{Z}(t)]}{\sqrt{2\pi V[\dot{Z}(0)]}} \int_{-\infty}^{0} e^{v} dv \frac{1}{\sqrt{2\pi V[Z(t)]}} e^{-\frac{u^2}{2V[Z(t)]}} \\
&= \sqrt{\frac{2}{\pi}} \sqrt{V[\dot{Z}(t)]} \frac{1}{\sqrt{2\pi V[Z(t)]}} e^{-\frac{u^2}{2V[Z(t)]}} \\
&= \frac{1}{\pi}\sqrt{\frac{V[\dot{Z}(t)]}{V[Z(t)]}} e^{-\frac{u^2}{2V[Z(t)]}} \\
&= \frac{1}{\pi}\sqrt{\frac{\lambda_2}{\lambda_0}} e^{-\frac{u^2}{2\lambda_0}}.
\end{aligned}$$

□

# B Theory of LMA

**Increment based convolution algorithm for simulation of LMA**

1. Pick $m$, and $dx$ so that $f(\cdots)$ is well approximated by its values on

$$-mdx < \cdots < -dx < 0 < dx < \cdots < mdx.$$

2. Pick $n \gg 2m+1$ in order to simulate the $n-2m$ values of the LMA process Z at frequency $dx^{-1}$.

3. Simulate $n$ identically and independently distributed (i.i.d.) $\Gamma(dx/\nu, 1)$ random variables and store them in a vector $G = [G_i]$.

4. Simulate $n$ i.i.d. zero mean standard normal random variables and store them in a vector $X$.

5. Compute $Y = f * (\sqrt{\nu G} \cdots X)$, where $\sqrt{\nu G} \cdots X = \sqrt{\nu G_i} \cdots X_i$, where $*$ denotes the operation of convolution and the simulated $n-2m$ values of $\int f(x-u)d\Lambda(u)$ are obtained from Y by discarding its first and last $m$ values.

The measure theory based definition of LMA process is given as follows:

**Definition 12** (Laplace moving average)**.** *For a Laplace measure $\Lambda$, controlled by a shift invariant measure $m$ and a kernel $f$ such that $\int f dm$ and $\int f 2dm$ are finite, the following process will be called a Laplace moving average(LMA):*

$$X_t = \int_x f(t-x)d\Lambda(x). \tag{B.1}$$

**Proposition 13** (Moments of the stochastic Laplace measure)**.** *Let $X = \int f d\Lambda$ and assume that $f^N \in L_2(\chi, \beta, m)$. Then the following recurrence formula for the moments holds*

$$\mathrm{E}[X^N] = (N-1)! \sum_{k=1}^{N} \frac{\mathrm{E}[X^{N-k}]}{(N-k)!} \int f^k dm S_{k-1} \tag{B.2}$$

*where*

$$S_r = \begin{cases} \sum_{k=0}^{\frac{r-1}{2}} s_{r,k}, & r \text{ is odd} \\ \mu(\frac{\sigma^2}{2})^{\frac{r}{2}} + \sum_{k=0}^{\frac{r}{2}-1} s_{r,k}, & r \text{ is even} \end{cases} \tag{B.3}$$

*and*

$$s_{r,k} = \mu^{r-2k-1} \left(\frac{\sigma^2}{2}\right)^k \left( \begin{pmatrix} r-k-1 \\ k \end{pmatrix} \sigma^2 + \begin{pmatrix} r-k \\ k \end{pmatrix} \mu^2 \right). \tag{B.4}$$

# C Estimation procedure of LMA and major MATLAB functions in use

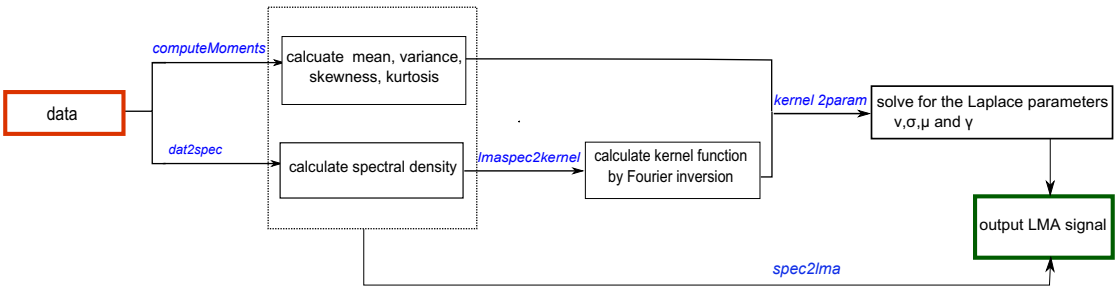


Figure 33: Simulation flow chart of LMA

First mean, variance, skewness and leptokurtic kurtosis are estimated from data by `computeMoments`. Then `dat2spec` calculates the spectral density from data and the output is used by `lmaspec2kernel` to estimate the kernel function by Fourier inversion. Finally Laplace parameters $\nu$, $\sigma$, $\mu$ and $\gamma$ are estimated by `kernel2param` with inputs of moments and kernel. Built on previous two commands, `spec2lma` generates a LMA signal in its output with inputs of spectral density and moments.

Major MATLAB functions:

- `computeMoments`: calculates the 1st to 4th moments of the signal. The outputs are mean, standard deviation, skewness and kurtosis.
- `dat2spec`: calculates the spectral density of the given signal.
- `lmaspec2kernel`: calculates the normalized symmetric kernel from spectral density based on formula (4.19). By normalized, we mean $\int f^2 d = 1$ where $f$ is the kernel function.
- `kernel2param`: computes the parameters $\nu, \sigma, \mu, \gamma$ in the LMA process with inputs kernel, skewness and kurtosis based on formulae (4.22) and (4.23).
- `spec2lma`: simulates a LMA process with inputs spectral density and moments.
- `computeDamage`: computes the rainflow damage estimation of a given signal. Input parameter 'k' varies according to the material and load kind under consideration.
- `dat2tp`: calculates turning points from signal. The output is two column matrix with times and turning points.
- `tp2lc`: computes the number of upcrossings from the turning points. The output is a two column matrix with levels and number of upcrossings.
- `tp2rfc`: finds the rainflow cycles from the sequence of turning points. The output is a two column matrix with rainflow minimums and paired maximums.

- `spec2sdat`: simulates a Gaussian process from given spectrum. The output is a two column matrix of times and simulated signal components.
- `spec2mom`: calculates spectral moments from spectrum.

## References


[1] Anders Bengtsson, Klas Bogsjö, and Igor Rychlik. Fatigue damage uncertainty. In *Robust design methodology for reliability: Exploring the Effects of Variation and Uncertainty*, pages 152–171. John Wiley& Sons, Ltd, 2009.

[2] Sofia Åberg and Krzysztof Podgórski. A class of non-gaussian second order random fields, 2008. Preprint2008, Department of Mathematical Sciences, Division of Mathematical Statistics, Chalmers University of Technology, University of Gothenburg, Göteborg Sweden.

[3] Klas Bogsjö. *Road Profile Statistics Relevant for Vehicle Fatigue.* PhD thesis, Mathematical Statistics, Centre for Mathematical Sciences, Lund University, 2007.

[4] Klas Bogsjö, Krzysztof Podgórski, and Igor Rychlik. Models for road surface roughness, 2010. Preprint2010, Department of Mathematical Sciences, Division of Mathematical Statistics, Chalmers University of Technology, University of Gothenburg, Göteborg Sweden.

[5] Harald Cramér and M. R. Leadbetter. *Stationary and Related Stochastic Processes: Sample Function Properties and Their Application.* Dover Publications, Mineola, New York, 2004.

[6] Masahiro Jono. Fatigue damage and crack growth under variable amplitude loading with reference to the counting methods of stress-strain ranges. *International Journal of Fatigue*, 27(8):1006–1015, 2005.

[7] Peter Mucka. Road waviness and the dynamic tyre force. *International Journal of Vehicle Design*, 36:216–232, 2004.

[8] Igor Rychlik. Cycle counting. preliminary version for *Encyclopedia of Tribology*, Springer.ed.

[9] Igor Rychlik. Five lectures on rainflow method. lecture notes of AMAS course on reliability-based design and optimisation, Warsaw, September 15-18, 2003.

[10] Igor Rychlik. Rain flow cycle distribution for fatigue life prediction under gaussian load processes. *Fatigue and Fracture of Engineering Material and Structures*, 10(3):251–260, 1987.

[11] Alfred A. Wolf. An ergodic theorem and its generalization. *Journal of the Franklin Institute*, 283(4):286–299, 1967.